EFL-3/E2F7 modulates Wnt signalling through repressing the LIT-1 Nemo-like kinase during asymmetric epidermal cell division in *Caenorhabditis elegans*.

Mar Ferrando-Marco[1] and Michalis Barkoulas[1]

[1]Department of Life Sciences, Imperial College, London SW7 2AZ, United Kingdom.

*Corresponding Author: m.barkoulas@imperial.ac.uk

Keywords *C. elegans*, E2F family, EFL-3/E2F7, asymmetric division, seam cell, Wnt signalling, LIT-1/NLK

Abstract

The E2F family of transcription factors is conserved in higher eukaryotes and plays pivotal roles in controlling gene expression during the cell cycle. Most canonical E2Fs associate with members of the Dimerisation Partner (DP) family to activate or repress target genes. However, atypical repressors, such as E2F7 and E2F8, lack DP interaction domains and their functions are less understood. We report here that EFL-3, the E2F7 homologue of *C. elegans*, regulates epidermal stem cell differentiation. We show that phenotypic defects in *efl-3* mutants depend on the Nemo-like kinase *lit-1.* EFL-3 represses *lit-1* expression through direct binding to a *lit-1* intronic element. Increased LIT-1 expression in *efl-3* mutants reduces POP-1/TCF nuclear distribution, and consequently alters Wnt pathway activation. Our findings provide a mechanistic link between an atypical E2F family member and NLK during *C. elegans* asymmetric cell division, which may be conserved in other animals.

Highlights

- EFL-3 is enriched in anterior daughter cells following asymmetric seam cell division.
- *efl-3* mutants show defects in cell differentiation and seam cell fate maintenance.
- EFL-3 directly represses *lit-1*/NLK expression.
- EFL-3-mediated *lit-1* repression alters POP-1 nuclear levels, linking EFL-3 to Wnt signalling.

Introduction

Development of multicellular organisms depends on the formation of different tissues and specialised cell types. Stem cells are central in this process having the potential to give rise to cellular diversity through asymmetric cell division, while they are maintained in an undifferentiated state and can increase their population through symmetric division[1]. The balance between symmetric and asymmetric divisions needs to be tightly regulated because defects in stem cell regulation can compromise tissue homeostasis and increase the risk of cancer[2,3]. Therefore, studying key genes and pathways regulating stem cell behaviour is central for unravelling mechanisms at play in healthy and disease state.

The epidermal seam cells of *Caenorhabditis elegans* serve as a model to study stem cell regulation[4]. Seam cells are linearly arranged throughout the length of the body (named H0-H2, V1-V6, and T) and divide symmetrically and asymmetrically in a stem-like manner during postembryonic development (Figure 1A). Following most seam cell asymmetric divisions, posterior daughter cells maintain the seam cell fate, whereas anterior daughter cells endoreduplicate and fuse to the hyp7 epidermal syncytium[5,6]. The seam cells generate the majority of the epidermal nuclei and thus the cuticle, which is essential for growth and protection from biotic and abiotic stress[7]. The H2, V5 and T seam cell lineages also give rise to neuronal precursors[5]. The seam cells expand their population from 10 to 16 through a symmetric division at the early L2 stage, when both daughter cells maintain the proliferative potential. At the end of larval development, the 16 seam cells terminally differentiate and fuse into another syncytium that generates the cuticle ridges called alae[8]. Seam cell divisions and their position along the anterior-posterior axis are highly invariant, allowing the characterisation of phenotypic errors at single-cell resolution[9].

Seam cell development is controlled by Wnt signalling, a widely conserved pathway consisting of intercellular signals that can travel in the body to shape tissues through influencing cell polarity and proliferation[10–12]. Correct seam cell patterning relies on the Wnt/β-catenin asymmetry pathway (WβA). This pathway ensures that following asymmetric division, posterior daughter cells activate Wnt targets and retain seam cell fate, while anterior daughter cells do not activate Wnt and instead differentiate[13,14]. In the dividing mother cell, Wnt ligands drive positive regulators such as Frizzled receptors and

77 Dishevelled to localise to the posterior cortex[15–17]. Instead, negative WβA regulators, such
78 as APR-1/APC and PRY-1/Axin asymmetrically localise to the anterior cortex[18,19]. The β-
79 catenin WRM-1 also localises to the anterior cortex and recruits more APR-1/APC and
80 PRY-1/Axin[19,20]. In turn, APR-1 promotes anterior nuclear export of WRM-1 through
81 regulation of microtubule dynamics, while absence of APR-1 from the posterior daughter
82 cell after division leads to nuclear WRM-1 localisation[17,21]. Moreover, cortical APR-1
83 promotes SYS-1/β-catenin degradation through the destruction complex, leading to
84 asymmetric localisation of SYS-1 to the posterior nucleus[18] In posterior daughter cells,
85 high nuclear WRM-1 binds to LIT-1 promoting its activation by MOM-4/MAPK and nuclear
86 translocation[20,22,23]. Nuclear LIT-1 phosphorylates POP-1, the sole Tcf/Lef homologue of
87 *C. elegans*, leading to its nuclear export[24–27]. Low POP-1 and high SYS-1 levels in
88 posterior daughter nuclei allow the formation of a TCF/β-catenin transcriptional activator
89 complex (POP-1/SYS-1) that activates Wnt targets[13,28–30], such as the GATA transcription
90 factor EGL-18 [31]. In anterior daughter cells, high POP-1 and low SYS-1 levels in the
91 nucleus lead to recruitment of corepressors and transcriptional repression of Wnt
92 targets[30,32]. Besides Wnt signalling, seam cell patterning is also regulated by other
93 conserved transcription factors, such as a Runx/CBFβ module, CEH-16/engrailed and
94 various GATA factors, which can influence the decision between stem cell fate
95 maintenance or differentiation[33–39]
96
97
98 The E2F family of transcription factors (E2F1-8 in humans) controls gene expression
99 during the cell cycle. E2F1-6 associate with DP proteins to form heterodimers that control
100 the expression of cell cycle genes[40,41]. Atypical E2F7-8 lack a DP binding domain and are
101 thought to act as transcriptional repressors[42–46]. Most E2Fs are regulated during the cell
102 cycle through direct binding to pocket proteins, such as the tumour suppressor RB. These
103 interactions are in turn regulated by the activity of cyclin-dependent kinase (CDK) and
104 cyclin complexes, which phosphorylate pocket proteins causing E2F release[40]. The CDK-
105 RB-E2F pathway is essential to prevent abnormal proliferation and tumour growth, with
106 unrestrained E2F-mediated transcription being a key driver for many cancers[47,48]. While

107 E2Fs have been largely studied in the context of cell division, it is known that they also
108 have non-canonical functions beyond the cell cycle [49,50]. The *C. elegans* genome contains
109 three homologs of the mammalian E2F family, *efl-1*, *efl-2* and *efl-3*. EFL-1 and EFL-2 bind
110 to DP/DPL-1 to repress expression of genes ensuring correct development of tissues
111 such as the vulva[41,51,52]. For example, *efl-1* participates in the DRM complex and the
112 SynMuvB gene regulatory pathway that inhibits vulval development and prevents somatic
113 cells from acquiring a germline fate[53,54]. In addition, *efl-1* and *efl-2* have been described
114 to have pro-apoptotic function in the germline[55].

115 In this study, we describe the role of EFL-3, the E2F7 homologue of *C. elegans,* in seam
116 cell development. We report that EFL-3 localises preferentially in anterior daughter cells
117 following asymmetric seam cell division and this localisation depends on Wnt-signalling.
118 Tissue-specific *efl-3* mutants display gains and losses of seam cells. These phenotypes
119 are dependent on the Nemo-like kinase *lit-1*, which we find to be a direct EFL-3 target.
120 Increase of *lit-1* expression reduces POP-1 levels in the seam cell daughter nuclei leading
121 to changes in seam cell fate specification. Our study therefore provides evidence that the
122 atypical E2F EFL-3 modulates epidermal stem cell patterning in *C. elegans* through
123 regulation of *lit-1* expression, and consequently Wnt signalling pathway activity.

124 **Results**

125 **EFL-3 shows an asymmetric distribution following seam cell division**

126 As part of our efforts to gain insights into the machinery regulating seam cell
127 development, we previously performed transcriptional profiling and identified *efl-3* as a
128 seam cell-expressed transcription factor[56]. The *C. elegans* genome contains three E2F
129 family members, *efl-1*, *efl-2* and *efl-3,* but only downregulation of *efl-3* led to a significant
130 change in the average number of seam cells (Figure 1B).

131 To characterise the *efl-3* expression pattern in the seam cells, we used single-
132 molecule fluorescence *in situ* hybridisation (smFISH). We focused on the V1-V4 lineages
133 that divide in a similar division pattern, and the L2 larval stage during which seam cells
134 divide twice, first symmetrically and then asymmetrically. Interestingly, we observed an
135 asymmetric localisation of *efl-3* transcripts between the two daughter cells following the

136 symmetric and asymmetric L2 divisions (Figure 1C and D). In both cases, anterior
137 daughter cells displayed a higher number of *efl-3* mRNA transcripts compared to posterior
138 daughters (Figure 1E). Following the L2 asymmetric cell division, posterior daughter cells
139 presented strong reduction in *efl-3* transcript abundance, with 50% of cells showing no
140 *efl-3* mRNAs at all (Figure 1E).

141 To assess whether this asymmetric mRNA distribution also reflected how EFL-3 is
142 distributed at the protein level, we generated and imaged an *efl-3::gfp* knock-in strain.
143 Consistent with the mRNA transcript enrichment in anterior cells, EFL-3::GFP expression
144 was moderately enriched in anterior daughter cells after symmetric division in comparison
145 to posterior daughters (Figure 1F and G). Following the L2 asymmetric division, this
146 enrichment became more pronounced, with EFL-3::GFP expression specifically observed
147 in anterior daughter cells (Figure 1H). We reasoned that the Wnt pathway that is normally
148 activated in posterior daughter cells retaining the seam cell fate may contribute to the *efl-*
149 *3* repression seen in posterior cells. To test this hypothesis, we knocked-down the Wnt
150 downstream effector *egl-18* by RNAi, which results in loss of seam cell fate maintenance
151 and decreased terminal seam cell number (Figure 1I). Notably, we found EFL-3::GFP to
152 be expressed in 21% of posterior daughter cells in *egl-18* RNAi animals compared to 0%
153 in the control treatment (Figure 1J). Taken together, these results highlight that EFL-3
154 distribution in seam cells is asymmetric and that this asymmetry is dependent on Wnt
155 pathway activation.

156 **Loss of *efl-3* function leads to gains and losses of seam cells during larval**
157 **development**

158 To consolidate the RNAi results, we sought to study the impact of strong loss of
159 *efl-3* function on seam cell development. To circumvent the fact that *efl-3* is an essential
160 gene[57], we constructed a seam cell-specific mutant by inserting *loxP* recombination sites
161 flanking the *efl-3* locus and introducing this modification into a genetic background
162 expressing Cre recombinase specifically in the seam cells. We confirmed that neither the
163 introduction of *loxP* sites flanking the *efl-3* locus nor the expression of Cre recombinase
164 in the seam cells disrupt seam cell development (Figure S1A). Furthermore, transgenic
165 *efl-3*^{loxP} animals carrying the Cre recombinase did not show any *efl-3* expression in the

166 seam cells by smFISH, hence they are likely to represent seam cell-specific null mutants
167 (Figure S1B). We found that tissue-specific *efl-3* mutants displayed a stronger phenotype
168 than *efl-3* RNAi treated animals, with both gains and losses of seam cells observed at the
169 early adult stage (Figure 2A and B). Gains of seam cells were more frequent in the H1p
170 and anterior V lineages (Figure 2C), whereas seam cell losses were more frequently
171 observed in the posterior V lineages (Figure 2D). When *efl-3* mutants were treated with
172 *egl-18* RNAi, the seam cell loss phenotype was enhanced (Figure S1C). Taken together,
173 these results suggest that EFL-3 can both promote and repress seam cell fate.

174 To determine at what larval stage seam cells are gained or lost in the *efl-3* mutant, we
175 carried out detailed lineage analysis during post-embryonic development. We found that
176 at the late L2 and late L3 stages, *efl-3* mutant animals only displayed seam cell gains
177 (Figure S1D, E and F). Gaps in the seam cell line were only observed later at the late L4
178 stage, as shown by the loss of expression of the epidermal marker *wrt-2p::GFP-PH*
179 (Figure S1G). Cells within these gaps also lacked expression of another seam cell marker,
180 the nuclear hormone receptor *nhr-73* by smFISH (Figure S1H). Therefore, lineage
181 analysis suggests that in *efl-3* mutant animals seam cell losses occur only following the
182 L4 asymmetric division and thus later than the onset of gains.

183 To characterise the developmental state of the anterior V1-V4 cells that retain the
184 expression of *SCM::GFP* following division, we investigated the expression pattern of
185 other transcription factors whose expression is known to correlate with seam cell fate,
186 such as *nhr-73*, *elt-1* and *egl-18.* In all cases, we found that *efl-3* mutants ectopically
187 expressed these genes in anterior daughter cells following asymmetric division (Figure
188 2E-G). In the case of *egl-18*, we confirmed this result at the protein level by studying the
189 expression of an endogenously tagged *egl-18* with *mNeonGreen*. We found a significant
190 increase in EGL-18 protein expression in anterior daughter cells in *efl-3* mutants
191 compared to control (Figure S1I and J).

192 Because E2Fs, including E2F7, are known to participate in the regulation of the cell cycle
193 [58,59], we asked whether the defects in cell differentiation in *efl-3* mutant animals may be
194 an indirect consequence of cell cycle perturbation. Lineage analysis did not reveal any
195 gross difference in the timing of cell division between wild-type and mutant. Furthermore,

196 it is known that following the L2 asymmetric division, anterior daughter cells
197 endoreduplicate before fusing to the hyp7 syncytium[8]. We found that *efl-3* mutants did not
198 show changes in endoreduplication in anterior nuclei (Figure S1K and L). Taken together,
199 these findings suggest that the observed phenotypes in *efl-3* mutants are more likely to
200 be linked directly to changes in cell differentiation.

201 **Identification of putative EFL-3 targets via NanoDam**

202 To identify downstream targets of EFL-3 in the seam cells, we used a modified
203 TaDa approach for streamlined tissue-specific transcription factor binding called
204 NanoDam[60,61]. NanoDam employs the main TaDa principle to overcome the considerable
205 toxicity observed when Dam-fusions are expressed at high levels in animal cells[35,62].
206 Briefly, transgenes are expressed at very low levels in the tissue of interest via a
207 bicistronic mRNA cassette design harbouring two open reading frames (ORFs). The first
208 ORF encodes a fluorescent protein and is followed by two STOP codons and a frameshift
209 mutation before the ATG of the second ORF. Because of the universal property of
210 eukaryotic ribosomes to reinitiate translation after a STOP codon at a reduced frequency,
211 this transgene configuration leads to low levels of Dam-Protein of interest fusion
212 production. NanoDam relies on the tissue-specific expression of a vhhGFP4 nanobody
213 fused to Dam. This allows profiling of putative targets at the desired tissue upon crossing
214 the GFP nanobody:Dam transgene to a TF-GFP transgenic line (here the *efl-3::gfp* knock-
215 in strain). We performed EFL-3 NanoDam at the L4 stage using both C-terminal and N-
216 terminal fusions of the Dam:GFP-nanobody transgene expressed in the seam cells. The
217 functionality of the EFL-3::GFP fusion was assessed by scoring the seam cell number in
218 heterozygous +*srf-3i::cre efl-3*^{loxP} / *efl-3::gfp* animals, which showed a wild-type seam cell
219 number similar to heterozygous +*srf-3i::cre efl-3*^{loxP}*/ wt* animals (Figure S2A)

220 Amplicons representing methylated genomic sequences were sequenced and data was
221 analysed using the damidseq pipeline[63]. EFL-3 NanoDam signal was calculated as log2
222 (EFL-3:GFP; Dam:GFP-nanobody / Dam:GFP-nanobody) ratio scores per GATC
223 fragment of the genome for each Dam:GFP-nanobody configuration. Aggregate genome-
224 wide signal profiles across genes containing statistically significant peaks between 5 kb
225 upstream of the transcriptional start site (TSS) and 2 kb downstream of the transcription

226 end site (TES) showed signal enrichment in sequences proximal to the TSS and the TES
227 (Figure S2B). We identified 1316 and 1237 statistically significant peaks in the case of
228 the C- and N-terminal Dam:GFP-nanobody fusions, respectively (Table S1), with > 70%
229 of peak overlap between the two datasets (Figure S2C). Hierarchical clustering of the
230 localization and score of those peaks that lie between 5 kb upstream and 2 kb
231 downstream of genes revealed clusters of signal enrichment upstream to TSS, within the
232 genes and downstream to TES regions (Figure S2D). Peaks were assigned to the closest
233 gene leading to 1882 and 1826 genes for each configuration with an 80% overlap
234 between the two gene datasets. The list of candidate EFL-3 target genes showed
235 significant overlap with genes expressed in seam cells based on sci-RNAseq data[64] and
236 with a filtered list of genes with known roles in seam cell development from the literature
237 (Table S2).

238 **EFL-3 controls *lit-1* expression in seam cells**

239 One potential target reproducibly identified in the NanoDam datasets was *lit-1*, which
240 encodes a MAP kinase homolog of the human NLK and is known to participate in Wnt
241 signal transduction by regulating the nuclear distribution of POP-1[20,24–27]. NanoDam
242 profiling revealed significant signal enrichment in the first intron of *lit-1* (Figure 3A). We
243 carried out *lit-1* smFISH to compare *lit-1* expression between wild type and *efl-3* mutants
244 after the L2 asymmetric division. We found a significant increase in *lit-1* transcript levels
245 in anterior and posterior daughter cells, suggesting that EFL-3 may act as a repressor of
246 *lit-1* expression in the seam cells (Figure 3B). Following an asymmetric seam cell division,
247 LIT-1 has been reported to localise preferentially to the nucleus of posterior daughter cells
248 where it phosphorylates POP-1 to trigger its nuclear export[20]. We therefore investigated
249 LIT-1 nuclear levels during symmetric and asymmetric L2 division using a *lit-1::gfp* knock-
250 in strain. Consistent with the smFISH results above, we found that LIT-1 levels were
251 significantly increased in *efl-3* mutant animals in anterior and posterior daughter cells
252 following symmetric and asymmetric division (Figure 3C and D, Figure S3A and B).

253 To address whether the increase in *lit-1* levels could be causative for the seam cell
254 phenotype observed in *efl-3* mutants, we carried out *lit-1* RNAi in the *efl-3* mutant
255 background. We found a significant reduction in the mean seam cell number of *efl-3*

256 mutant animals upon *lit-1* RNAi treatment compared to the control treatment (Figure 3E).
257 Detailed lineage analysis revealed that this reduction in seam cell number was driven by
258 a statistically significant suppression of seam cell gains in anterior V lineages in *efl-3*
259 mutants (Figure S3C). Furthermore, we found a statistically significant reduction in
260 posterior V lineage cell losses in *efl-3* mutants treated with *lit-1* RNAi (Figure S3D), which
261 was masked when looking at the aggregate seam cell number counts. The suppression
262 of seam cell gains and losses observed in *efl-3* mutants suggests that both phenotypes
263 are LIT-1-dependent.

264 To test whether EFL-3 could directly control the expression of *lit-1* through the identified
265 site on the first intron, we used CRISPR-mediated genome editing to delete the entire
266 EFL-3 NanoDam peak (Figure 3A). Animals containing this intronic deletion showed an
267 increase in nuclear LIT-1 levels in anterior daughter cells following the asymmetric L2
268 division (Figure 3C and D). We note that this increase was lesser in magnitude than what
269 is observed in *efl-3* mutants, suggesting that this intronic element may not be the only
270 way via which EFL-3 controls *lit-1* expression in the seam cells. Consistent with this
271 hypothesis, *efl-3* RNAi was found to further increase LIT-1 levels in animals carrying the
272 intronic deletion. This further suggests that EFL-3 is likely to regulate *lit-1* expression
273 directly through additional regulatory elements or indirectly through other intermediate
274 transcription factors (Figure S3E and F).

275 **Decrease in nuclear POP-1 levels correlates with seam cell gains and losses in *efl-***
276 ***3* mutants**

277 LIT-1 accumulation in the nucleus of posterior daughter cells is predicted to cause POP-
278 1 nuclear export, thereby ensuring an optimal β-catenin (SYS-1) / POP-1 ratio in the
279 nucleus that is conductive to Wnt target activation[20,28–30]. Low LIT-1 levels in the nuclei of
280 anterior daughter cells allow POP-1 to also remain at high levels in the nucleus and
281 associate with proteins repressing Wnt target genes[30,32]. We therefore asked whether
282 higher LIT-1 levels in *efl-3* mutant nuclei have a consequence on POP-1 localisation. To
283 test this prediction, we studied nuclear POP-1 protein levels upon loss of *efl-3* function
284 using a *gfp::pop-1* knock-in strain. In wild-type animals, POP-1 levels were lower in
285 posterior daughter cells in comparison to anterior daughter cells following the L2

286 asymmetric division (Figure 4A and B). In *efl-3* mutant animals, we found a significant
287 decrease in POP-1 levels in both anterior and posterior daughter cells (Figure 4A and B).
288 Changes in POP-1 expression were at the protein level because *pop-1* mRNA transcripts
289 were unchanged between control and *efl-3* RNAi-treated animals (Figure S4A and B). We
290 also compared POP-1 nuclear levels at the L2 and L4 stages. In wild type animals, POP-
291 1::GFP expression was higher at the L4 stage compared to L2 (Figure S4C and D).
292 Additionally, we observed a less pronounced asymmetry between anterior and posterior
293 daughter cells at the L4 stage. (Figure S4E). POP-1 levels were reduced to a similar
294 average level in *efl-3* mutants at both the L2 and L4 stages (Figure S4 C and D). These
295 results suggest that while reduction in POP-1 levels can readily explain the seam cell
296 gains observed in *efl-3* mutants, absolute POP-1 levels alone cannot explain the seam
297 cell losses observed specifically at L4.

298 To test whether increase in *lit-1* expression can explain the seam cell losses observed in
299 *efl-3* mutants, we overexpressed *lit-1* under the *arf-5i* element, which predominantly
300 drives expression in posterior daughters retaining seam cell fate[65]. Animals
301 overexpressing *lit-1* presented losses of seam cells leading to a significant decrease in
302 the mean seam cell number (Figure 4C). Similar to *efl-3* mutants, losses of seam cells
303 were predominantly observed after the L4 asymmetric division (Figure 4C and D). As we
304 found comparable L2 and L4 POP-1 levels in posterior daughter cells of *efl-3* mutants,
305 we hypothesised that the losses observed at L4 may reflect an increased sensitivity to
306 change. To test this hypothesis further, we investigated seam cell defects in a strain
307 carrying the hypomorphic *pop-1(hu9)* allele and observed gains of seam cells leading to
308 a significant increase in the mean seam cell number (Figure S4F). Seam cell gains were
309 only observed at the L4 stage (Figure S4G), suggesting that seam cells are likely to
310 present a higher sensitivity to both gains and losses at this late larval stage.

311 **Discussion**

312 The E2F family of transcription factors are important for many cellular processes,
313 including cell cycle regulation, apoptosis, and DNA damage[50,66–68]. Atypical E2Fs are
314 known to act as transcriptional repressors antagonising canonical E2F activators[69–71]. For
315 example, E2F7 has been implicated in restraining cell proliferation in human cells via

316 directly regulating the expression of genes that regulate mitotic progression among other
317 targets, such as microRNAs[45,58,72,73]. Previous work on *efl-3* in *C. elegans* suggested a
318 role in preventing apoptosis in PVA and PVB neurons of the ventral nerve cord by
319 repressing the expression of the pro-apoptotic gene *egl-1*[57]. In addition, *efl-3* has been
320 implicated in the development of the somatic gonad by specifying the correct amount of
321 distant tip cells[74]. However, the exact molecular mechanisms of how this is achieved still
322 need to be elucidated. We report here that EFL-3 regulates asymmetric divisions in the
323 *C. elegans* epidermal stem cell model. Consistent with a role as a transcriptional
324 repressor, we show that EFL-3 represses *lit-1* expression in seam cells partially through
325 direct binding to an intronic element, which has a knock-on effect on POP-1 distribution.
326 Our study therefore reveals a link between an atypical E2F repressor and NLK-mediated
327 regulation of Wnt signalling in the context of asymmetric cell division.

328 We characterised the *efl-3* expression pattern at the mRNA and protein level and report
329 an enrichment in anterior seam cell daughters after symmetric and asymmetric divisions.
330 This enrichment profile is consistent with a role for EFL-3 in facilitating cell differentiation
331 of anterior daughter cells. While this function may be key to asymmetric cell division, it
332 could be bypassed during symmetric division similar to how Wnt asymmetry is also
333 masked at the phenotypic level[75]. Expression of atypical E2Fs is known to be cell cycle-
334 dependent, often with a maximum expression at the S phase[45,76] Following seam cell
335 asymmetric division, anterior daughters immediately proceed to S phase before fusing to
336 the hyp7 syncytium and differentiate, whereas the cell cycle progresses more slowly in
337 posterior daughter cells that will continue to divide[77] This difference in cell cycle
338 commitment between the two daughter cells could therefore contribute to the higher *efl-*
339 *3* expression found in anterior daughter cells after asymmetric division. However, it is
340 unlikely to be the main driver because a similar anterior *efl-3* enrichment was observed
341 following the symmetric division when both daughter cells progress simultaneously to S
342 phase[77] We propose that the anterior enrichment is likely driven by Wnt-dependent
343 repression in posterior daughter cells following an asymmetric cell division. This is
344 reminiscent of the atypical E2F7 repression by Wnt signalling reported in proliferating
345 hepatocytes[78]. Similar to *efl-3* mRNA distribution, *pop-1* transcription was also found to
346 be stronger in anterior daughter cells post-division, which may also reflect negative

347 feedback from Wnt activation on *pop-1* expression. Our findings indicate that besides the
348 known regulation of the LIT-1 - POP-1 axis at the protein level[22,23], transcriptional
349 regulation further safeguards seam cell fate decisions.

350 NLK-mediated Tcf/Lef phosphorylation can have positive or negative consequences on
351 its activity depending on the cellular context[79–81]. In *C. elegans*, LIT-1 promotes POP-1
352 nuclear export allowing low nuclear POP-1 levels in posterior daughter cells and Wnt
353 signalling activation[24–27]. In *efl-3* mutants, we found higher levels of nuclear LIT-1 and a
354 reduction in nuclear POP-1 levels in both anterior and posterior daughter cells following
355 asymmetric division. LIT-1 activity is regulated by WRM-1 and MOM-4. WRM-1 promotes
356 LIT-1 autophosphorylation, facilitates phosphorylation by MOM-4 and it's essential for LIT-
357 1 translocation to the nucleus[22,23]. This suggests that MOM-4 and WRM-1 activities are
358 sufficient to handle the increased amounts of LIT-1 in *efl-3* mutants. A decrease in POP-
359 1 levels has been shown to lead to ectopic Wnt signalling activation in anterior daughter
360 cells and subsequent symmetrisation of seam cell divisions[11]. Following asymmetric
361 division, posterior daughter cells require low levels of nuclear POP-1 to maintain the seam
362 cell fate. However, if levels of POP-1 drop below a threshold, seam cell fate can no longer
363 be maintained[75]. Therefore, changes in POP-1 nuclear levels through increased *lit-1*
364 expression may contribute to both the seam cell gains and losses observed in *efl-3*
365 mutants. (Figure 4E). In this scenario, lowering POP-1 levels in anterior daughter cells
366 where levels are normally high can activate Wnt targets and prevent cell differentiation.
367 Meanwhile, lowering POP-1 in posterior daughter cells that normally experience low POP-
368 1 levels can lead to premature differentiation (Figure 4E). While changes in POP-1 levels
369 could contribute to both seam cell gains and losses, our results demonstrate that absolute
370 POP-1 levels alone cannot fully explain the *efl-3* mutant phenotypes, particularly the loss
371 of seam cells at the L4 stage. These losses may rely upon additional sensitisation of seam
372 cells to changes in POP-1 levels at this developmental stage. Such sensitisation may
373 stem from changes in the abundance or distribution of Wnt signalling components
374 between the daughter cells as animals progress through development. For example, the
375 negative regulator PRY-1 has been reported to be more widely distributed in seam cells
376 at the L4 stage in comparison to earlier developmental stages[82]. Alternatively,
377 sensitisation to changes in POP-1 levels may also depend on interactions between spatial

patterning machinery in seam cells and the heterochronic pathway defining temporal identities[83,84].

E2F-mediated regulation of proliferation and Wnt signalling are fundamental pathways in healthy development with important implications in disease such as cancer[47,48,85]. However, the exact crosstalk between E2Fs and Wnt signalling is not well understood. One study recently reported that atypical E2F8 knockdown inhibits the Wnt signalling pathway in ovarian cancer cells[86]. Canonical E2F1 is also known to activate expression of axin2, inhibiting Wnt signalling to promote cell death in mammalian cells [87]. E2F1 has been shown to activate the expression of the Wnt receptor Frizzled in human osteoblasts to facilitate cell differentiation[88]. Our findings add to these reports by providing a mechanistic link between EFL3/E2F7 and the NLK-Tcf/Lef pathway in the context of epidermal stem cell fate determination in *C. elegans*. Besides TCF, NLK phosphorylates many other substrates so a link between E2F7 and NLK may have broader implications for vertebrate and invertebrate development.

Figure legends

Figure 1. EFL-3 is an E2F transcription factor regulating seam cell development.

(A) Schematic showing seam cell divisions from L1 to L4. Seam cells are labelled in green, hypodermal cells are labelled in grey and neuroblasts are labelled in purple. **(B)** Seam cell number counts upon RNAi targeting members of the E2F family in *C. elegans*. Unlike *efl-1* and *efl-2*, downregulation of *efl-3* leads to a significant increase in the terminal seam cell number ($p<0.001$ with a t-test, $n = 30$). **(C-D)** Representative *efl-3* smFISH images following the L2 symmetric division (C), and the L2 asymmetric division (D). Seam cell nuclei are labelled using *SCM::GFP*. **(E)** Quantification of *efl-3* mRNA spots in V1-V4 seam cells before (p) and after the L2 symmetric division (pa, pp), and following the L2 asymmetric division (paa, pap, ppa, ppp), $36 \leq n \leq 166$. **(F)** Representative image of EFL-3::GFP before the L2 asymmetric division. **(G)** Quantification of EFL-3::GFP fluorescence intensity before the L2 asymmetric division in V1-V4 lineages. Anterior cells show higher amounts of EFL-3 compared to posterior cells ($p<0.01$ with a t-test, $n = 45$). **(H)**

407 Representative image of EFL-3::GFP after the L2 asymmetric division. **(I)** *egl-18* RNAi-
408 treated animals show a statistically significant decrease in the mean seam cell number
409 (p<0.001 with a t-test) compared to control animals, n = 41. **(J)** Posterior daughter cells
410 (marked with red arrowhead) show expression of EFL-3::GFP when treated with *egl-18*
411 RNAi following the asymmetric L3 division, n = 91. Blue arrowheads in D and H point to
412 anterior daughter cells. In F, H and J the membrane of the seam cells is labelled using
413 the apical junction marker *ajm-1p::mCherry*. Error bars in B, E, G and I show the mean ±
414 standard deviation. Scale bars are 5μm in C, D, F, H and J.

415 **Figure 2. A tissue-specific *efl-3* mutant displays gains and losses of seam cells. (A)**
416 Representative images of tissue-specific *efl-3* mutant animals (+*srf-3i::cre efl-3*^{loxP}) versus
417 controls (-*srf-3i::cre efl-3*^{loxP}) at the early adult stage. Blue brackets indicate lineages with
418 seam cell gains, red arrowheads point to lineages with seam cell losses. **(B)** Seam cell
419 counts in tissue-specific *efl-3* mutant animals show a significant increase in the average
420 number of seam cells in comparison to controls (p<0.001 with a t-test, 58 ≤ n ≤ 64). Error
421 bars show the mean ± standard deviation. **(C-D)** Heatmaps showing frequency of seam
422 cell gains (C) and losses (D) per cell lineage at the end of postembryonic development in
423 tissue-specific *efl-3* mutant animals versus controls (n = 50 per condition, a = anterior
424 lineage, p = posterior lineage). **(E-G)** Representative smFISH images of *nhr-73* (E), *elt-1*
425 (F) and *egl-18* (G) mRNA distribution in tissue-specific *efl-3* mutant animals in comparison
426 to controls following the L2 asymmetric division. Blue arrowheads point to anterior
427 daughter cells that ectopically express *nhr-73*, *elt-1* and *egl-18* in *efl-3* mutant animals.
428 Seam cell nuclei are labelled using *SCM::GFP*. Scale bars are 50 μm in A and 5μm in E-
429 G. See also Figure S1.

430 **Figure 3. EFL-3 directly represses *lit-1* expression. (A)** Signal profiles for C-terminal
431 (blue) and N-terminal (red) NanoDam reflecting EFL-3::GFP binding near the *lit-1* locus.
432 The y axis represents $\log_2$(EFL-3::GFP; GFP-nanobody:dam /GFP-nanobody:dam) score
433 and the scale bar length is 1 kb. Statistically significant peaks are indicated by lightly
434 shaded rectangles on the signal tracks (FDR < 0.05). The generated *lit-1(icb164)* CRISPR
435 deletion is shown in orange. **(B)** Quantification of *lit-1* mRNA spots in V1-V4 lineages in
436 anterior and posterior daughter cells in *efl-3* tissue-specific mutants (+*srf-3i::cre efl-3*^{loxP})

437 versus controls (-*srf-3i::cre efl-3*^{loxP}) following the L2 asymmetric division, 100≤ n ≤ 126
438 per condition. **(C)** Representative images of LIT-1::GFP following the L2 asymmetric
439 division in controls (-*srf-3i::cre efl-3*^{loxP}), tissue-specific *efl-3* mutants (+*srf-3i::cre efl-3*^{loxP})
440 and animals containing the *lit-1(icb164)* CRISPR deletion. Seam cell nuclei are circled in
441 white. Hypodermal nuclei are labelled with blue arrowheads, a = anterior daughter cell, p
442 = posterior daughter cell. **(D)** Quantification of LIT-1::GFP fluorescence intensity in the
443 nuclei of V1-V4 seam cells following the L2 asymmetric division in controls (-*srf-3i::cre*
444 *efl-3*^{loxP}), tissue-specific *efl-3* mutants (+*srf-3i::cre efl-3*^{loxP}) and animals containing the *lit-*
445 *1(icb164)* CRISPR deletion; n ≥ 175. **(E)** Seam cell counts in *efl-3* tissue-specific mutant
446 animals versus controls treated with *lit-1* RNAi or empty vector; n = 50 per condition. Error
447 bars in B, D and E show the mean ± standard deviation and **** represent p<0.001 and
448 ** p<0.01 with a t-test.. Scale bars are 5 μm in C. See also Figures S2 and S3.

449 **Figure 4. *efl-3* mutants show changes in POP-1 nuclear distribution that are**
450 **compatible with seam cell gains and losses. (A)** Representative images of GFP::POP-
451 1 following the L2 asymmetric division in tissue-specific *efl-3* mutant animals (+*srf-3i::cre*
452 *efl-3*^{loxP}) versus controls (-*srf-3i::cre efl-3*^{loxP}). Blue arrowheads indicate cells with visually
453 lower expression of GFP::POP-1. Scale bars are 5 μm. **(B)** Quantification of GFP::POP-
454 1 fluorescence intensity following the L2 asymmetric division in tissue-specific *efl-3*
455 mutant animals versus controls, n ≥ 294. **** p<0.001 with a t-test. **(C)** Seam cell counts
456 in wild-type (-*icbEx707*) and animals overexpressing *lit-1* under the *arf-5i* element
457 (+*icbEx707*) at the late L2, late L3 and late L4 stages. At late L4, +*icbEx707* present a
458 significant decrease in the average number of seam cells compared to wild-type (**p<0.01
459 with a t-test), n = 36. **(D)** Heatmap showing frequency of seam cell losses per cell lineage
460 at the late L2, late L3 and late L4 stages in wild-type (-*icbEx707*) and in animals
461 overexpressing *lit-1* (+*icbEx707*), n = 36 per condition, a = anterior lineage, p = posterior
462 lineage. **(E)** Model of Wnt signalling activation in wild-type and in *efl-3* mutant animals. In
463 wild-type animals, anterior daughters present high POP-1 nuclear levels leading to
464 repression of Wnt target genes and differentiation. Posterior daughter cells exhibit POP-
465 1 nuclear export thanks to LIT-1 and WRM-1 activities. POP-1 interacts with SYS-1 to
466 drive expression of Wnt target genes resulting in seam cell fate maintenance. In *efl-3*
467 mutants, nuclear LIT-1 levels increase in both daughter cells leading to increased POP-1

468 nuclear export. As a consequence, in L2, L3 and L4 divisions anterior daughter cells show
469 ectopic activation of the Wnt signalling causing gains of seam cells. Because of additional
470 sensitisation, in L4 divisions some posterior daughter cells fail to activate the Wnt
471 signalling and lose seam cell fate. Fz = Frizzled; DS = Dishevelled; W = WRM-1; S =
472 SYS-1; co-R = POP-1 co-repressors. Frizzled and dishevelled localise to the posterior
473 cortex where they bind the Wnt ligand (Wnt). APC (APR-1), Axin (PRY-1), WRM-1 and
474 LIT-1 localise to the anterior cortex. Error bars in B and C show the mean ± standard
475 deviation. See also Figure S4.

476 **Supplementary Material**

477 **Figure S1: Phenotypic characterisation of *efl-3* mutants. (A)** Seam cell counts in wild-
478 type *(-srf-3::cre*), animals expressing the CRE recombinase in the seam cells (+*srf-3::cre*)
479 and animals with *efl-3* locus floxed, n ≥ 30. **(B)** Representative images of *efl-3* smFISH
480 following the L2 asymmetric division in wild-type (*-srf-3::cre efl-3*^{loxP}) and in *efl-3* mutant
481 animals (+*srf-3::cre efl-3*^{loxP}). Seam cell nuclei are labelled using *SCM::GFP* and the
482 apical junction marker *AJM-1p::GFP. +srf-3::cre* animals don't show *efl-3* mRNA spots in
483 the seam cells. Red arrowheads point to *efl-3* mRNA spots in the hypodermis. **(C)** Seam
484 cell counts in wild-type and *efl-3* mutant animals treated with control and *egl-18* RNAi.
485 Error bars show the mean ±standard deviation, n ≥ 46 per condition. **(D)** Representative
486 images of seam cells at the late L2 stage in wild type and in *efl-3* mutant animals. Seam
487 cells are labelled with the epidermal marker *wrt-2p::GFP::PH; wrt-2p::GFP::H2B*. Blue
488 arrowheads indicate anterior daughter cells that failed to differentiate following
489 asymmetric division. **(E)** Heatmaps showing frequency of seam cell gains per cell lineage
490 at the late L2 and late L3 stages in wild-type and in *efl-3* mutant animals. No seam cell
491 losses were observed in any of these stages, n ≥ 30 per condition, a = anterior lineage, p
492 = posterior lineage. **(F)** Seam cell counts in wild-type and *efl-3* mutant animals at the late
493 L2 and late L3 stages. *efl-3* mutants present a significant increase in the average number
494 of seam cells compared to wild-type. **(G)** Representative images of the seam cells at L4
495 stage in wild-type (*-srf-3::cre efl-3*^{loxP}) and in *efl-3* mutant animals (+*srf-3::cre efl-3*^{loxP}).
496 Seam cells are labelled with the epidermal marker *wrt-2p::GFP::PH; wrt-2p::GFP::H2B*.
497 **(H)** Representative *nhr-73* smFISH images at L4 stage in wild-type (*-srf-3::cre efl-3*^{loxP})

498 and in *efl-3* mutant animals (+*srf-3::cre efl-3*^{loxP}). In G and H, *efl-3* mutants present gaps
499 in the seam cell line indicated with a red bracket. **(I)** Representative images of EGL-
500 18::mNeonGreen following the L2 asymmetric division in wild-type (-*srf-3::cre efl-3*^{loxP})
501 and in *efl-3* mutant animals (+*srf-3::cre efl-3*^{loxP}). Blue arrowheads indicate representative
502 anterior daughter cells with higher expression of EGL-18::mNeonGreen. **(J)**
503 Quantification of EGL-18::mNeonGreen following the L2 asymmetric division in wild-type
504 (-*srf-3::cre efl-3*^{loxP}) and in *efl-3* mutant animals (+*srf-3::cre efl-3*^{loxP}), n ≥ 100. **(K)**
505 Representative images of DAPI staining following L2 asymmetric division in wild-type (-
506 *srf-3::cre efl-3*^{loxP}) and in *efl-3* mutant animals (+*srf-3::cre efl-3*^{loxP}). Seam cell nuclei are
507 labelled with red arrowheads. **(L)** Quantification of DAPI fluorescence intensity in anterior
508 and posterior daughter cells following L2 asymmetric division in wild-type and *efl-3* mutant
509 animals, n ≥ 66. Error bars in A, C, F, J and L show the mean ±standard deviation. Scale
510 bars are 5 μm in B, D, G, H, I and K. In C, F, J and L, **** p<0.001 with a t-test.

511 **Figure S2: NanoDam analysis of EFL-3::GFP binding. (A)** Seam cell counts in *efl-3*
512 mutants, and in the F1 progeny of *efl-3* mutants crossed with WT or with *efl-3::gfp*
513 animals. Rescue of the phenotype demonstrates the functionality of the EFL-3::GFP
514 fusion. Cross progeny was identified via expression of the apical junction marker *ajm-*
515 *1p::mCherry*, **** p<0.001 with a t-test. **(B)** Aggregation plots of profiling data generated
516 by EFL-3 NanoDam showing average enrichment scores in 10-bp bins for regions of
517 equal length across all genes containing statistically significant peaks. Enrichment is seen
518 upstream and downstream of gene regions. Plots show 5 kb upstream of the transcription
519 start site (TSS) and 2 kb downstream of the transcription end site (TES). Gene bodies
520 are condensed into a 2 kb pseudo-length. Shaded areas represent 95% confidence
521 intervals. **(C)** Venn diagram of all call peaks between EFL-3 C- and N-terminal NanoDam.
522 P value was calculated by Monte Carlo simulations for significance of overlap between
523 datasets. **(D)** Heatmaps representing the hierarchically clustered localization and
524 enrichment score of all statistically significant peaks (FDR < 0.05) within 5 kb upstream
525 and 2 kb downstream of genes containing peaks.

526 **Figure S3: EFL-3 regulates LIT-1 levels and *lit-1* downregulation reduces the gains**
527 **and losses of seam cells observed in *efl-3* mutants. (A)** Representative images of LIT-

528 1::GFP at late L1 stage and following the L2 symmetric division in wild-type (*-srf-3::cre*
529 *efl-3*^{loxP}) and *efl-3* mutant animals (*+srf-3::cre efl-3*^{loxP}) **(B)** Quantification of LIT-1::GFP
530 fluorescence intensity in the nuclei of V1-V4 seam cells at late L1 and after the L2
531 symmetric division. LIT-1::GFP is significantly increased in anterior and posterior
532 daughter cells in *efl-3* mutant animals (*+srf-3::cre efl-3*^{loxP}) compared to wild-type animals
533 (*-srf-3::cre efl-3*^{loxP}) after the L2 symmetric division, 31 ≤ n ≤ 47. **(C-D)** Heatmaps showing
534 frequency of seam cell gains **(C)** and losses **(D)** per cell lineage at the end of
535 postembryonic development in wild-type (*-srf-3::cre efl-3*^{loxP}) and in *efl-3* mutant animals
536 (*+srf-3::cre efl-3*^{loxP}) treated with control and *lit-1* RNAi. Chi-square test was performed
537 for the pooled cell lineages highlighted in the red square in C and blue square in D. *
538 p<0.05, **** p<0.001. In C and D, n = 50 per condition. **(E)** Representative images of LIT-
539 1::GFP following the L2 asymmetric division in wild-type and *lit-1(icb164)* animals treated
540 with control and *efl-3* RNAi. **(F)** Quantification of LIT-1::GFP fluorescence intensity in the
541 nuclei of V1-V4 seam cells following the L2 asymmetric division. LIT-1::GFP is
542 significantly increased in anterior daughter cells in *efl-3* RNAi-treated animals compared
543 to control animals. Animals containing *lit-1(icb164)* CRISPR deletion didn't show further
544 increase in LIT-1::GFP fluorescence intensity in anterior daughter cells compared to wild-
545 type when treated with *efl-3* RNAi, 35 ≤ n ≤ 74. In A and E, seam cell nuclei are circled in
546 white, hypodermal nuclei are labelled with blue arrowheads, a = anterior daughter cell
547 and p = posterior daughter cell and scale bars are 5 μm. Error bars in B and F show the
548 mean ±standard deviation. **** p<0.001 with a t-test.

549 **Figure S4: *efl-3* mutants show changes in POP-1 nuclear distribution at L2 and L4**
550 **stage. (A)** Representative *pop-1* smFISH images after the L2 asymmetric division upon
551 *efl-3* RNAi compared to control treatment. Seam cells are labelled using *SCM::GFP*. **(B)**
552 Quantification of *pop-1* mRNA spots in V1-V4 lineages in anterior and posterior daughter
553 cells following the L2 asymmetric division in the conditions of A, 108 ≤ n ≤ 174. **(C)**
554 Representative images of GFP::POP-1 following the L2 and L4 asymmetric divisions in
555 tissue-specific *efl-3* mutant animals (*+srf-3i::cre efl-3*^{loxP}) versus wild-type (*-srf-3::cre efl-*
556 *3*^{loxP}). **(D)** Quantification of GFP::POP-1 fluorescence intensity following the L2 and L4
557 asymmetric divisions in tissue-specific *efl-3* mutant animals (*+srf-3i::cre efl-3*^{loxP}) versus
558 wild type (*-srf-3::cre efl-3*^{loxP}), 36 ≤ n ≤ 65. * *p*<0.05 and **** *p*<0.001 with a t-test. **(E)**

559 Anterior-posterior GFP::POP-1 ratios following the L2 and L4 asymmetric divisions in
560 tissue-specific *efl-3* mutant animals versus wild type, 36 ≤ n ≤ 65. **** $p<0.001$ with a t-
561 test. **(F)** Seam cell counts in wild-type and *pop-1(hu9)* mutant animals at the late L2, late
562 L3 and late L4 stages. At late L4, *efl-3* mutants present a significant increase in the
563 average number of seam cells compared to wild type, n = 36. **(G)** Heatmap showing
564 frequency of seam cell gains per cell lineage at the late L2, late L3 and late L4 stages in
565 wild-type and in *pop-1(hu9)* mutant animals., n = 36 per condition, a = anterior lineage, p
566 = posterior lineage. Error bars in B, D, E and F show the mean ± standard deviation.
567 Scale bars in A and C are 5 μm.

568 **Table S1:** List of statistically significant EFL-3 NanoDam peaks.

569 **Table S2:** List of putative EFL-3 target genes in seam cells.

570 **Table S3**: List of smFISH probes used in this study.

571

572 **STAR METHODS**

573 **KEY RESOURCES TABLE**

574 In an excel

575 **RESOURCE AVAILABILITY**

576 **Lead contact**

577 Further information and requests for reagents should be directed to and will be fulfilled by
578 the lead contact Michalis Barkoulas (m.barkoulas@imperial.ac.uk).

579 **Materials availability**

580 Plasmids and strains generated in this study are available upon request to the lead
581 contact.

582 **Data and code availability**

583 **EXPERIMENTAL MODEL AND STUDY PARTICIPANT DETAILS**

584 ***C. elegans* maintenance and genetics**

585 All *C. elegans* strains in this study were maintained at 20°C on Nematode Growth Medium
586 (NGM) plates seeded with *E. coli* OP50[89]. A list of strains used in this study is provided in
587 the Key Resources Table.

588 **METHOD DETAILS**

589 **Molecular Cloning and transient transgenesis**

590 To construct seam cell CRE expression vector pHIN32, *C. elegans* codon-optimised
591 woCre recombinase gene was amplified from pDK56 with oligos Wcre_F and Wcre_R
592 from pDK56. The amplicon was inserted by Gibson Assembly into pDK70 containing *srf-*
593 *3i* promoter. pHIN32 was injected into *efl-3* floxed animals at 5 ng/µl with 5 ng/µL *myo-*
594 *2::dsRed* as co-injection marker and 90 ng/µl BJ36 as carrier DNA.

595 To overexpress *lit-1* using the last intron of *arf-5* (*arf-5i*), *lit-1*^{d} fragment was amplified from
596 PHX7906 cDNA using the oligos (pes10)_lit-1_Fw and (unc54)_lit-1_Rv. The amplicon
597 was inserted by Gibson Assembly into pIR5 to create pMFM20. pMFM20 was injected
598 into JR667 at 20 ng/µl with 5 ng/µL *myo-2::dsRed* as co-injection marker and 85 ng/µl
599 BJ36 as carrier DNA.

600 **RNAi feeding**

601 RNAi by feeding was performed using *E. coli* HT115 expressing double-stranded RNA
602 corresponding to the target gene or the control dsRNA plasmid (empty vector) as food
603 source [90]. Bacteria cultures were grown overnight and 300 µl were seeded onto NGM
604 plates containing 25 µg/ml ampicillin, 12.5 µg/ml tetracyclin and 1 mM IPTG. All RNAi
605 treatments were performed during the postembryonic development by seeding eggs from
606 the corresponding strain onto the RNAi plates. RNAi bacteria clones used in this study
607 are from the commercially available Ahringer RNAi Library[91] (Source Bioscience).

608 **Stable transgenesis and CRISPR genome editing**

609 The endogenous copy of both *efl-3* and *lit-1* was tagged with codon optimized GFP and
610 the auxin-inducible degradation (AID) domain just before the stop codon at the C-terminus
611 using a CRISPR/Cas-9 approach (Suny Biotech).

612 *LoxP* sites flanking the *efl-3* endogenous locus (178 bp upstream of the transcription start
613 site and 351 bp downstream of the 3'UTR) were introduced by injecting JR667 animals
614 with 0.25 ng/µL protein Cas-9, 2.25 µM tracrRNA, 2.38 µM of 5'_efl-3_crRNA and 3'_efl-
615 3_crRNAs, 5.5 µM of 5' and 3' repair templates and 5 ng/µL *myo-2::dsRed*. crRNAs
616 targeted 241 bp upstream the TSS and 298 bp downstream the TES. 5' and 3' *efl-3* repair
617 templates presented 50 bp homology to either side of the Cas-9 cut site and included a
618 *loxP* sequence, a ClaI cut site and a M13uni_43 or M13rev_49 sequence, respectively.
619 Transgenic animals with red pharynx were genotyped using the oligos efl-3_5p_F, R and
620 efl-3_3p_F, R for 5' and 3' modification, respectively. The PCR product was digested with
621 ClaI restriction enzyme to confirm successful homologous repair.

622 To delete the predicted EFL-3 binding region on *lit-1* locus, PHX7906 animals were
623 injected with 0.25 ng/µL protein Cas-9, 2.25 µM tracrRNA, 2.38 µM of 5'_lit-1_crRNA and
624 3'_lit-1_crRNA and 5 ng/µL *myo-2::dsRed.* crRNAs targeted a 2743 bp long region inside
625 *lit-1d* first intron. Transgenic animals with red pharynx were screened for the presence of
626 the deletion using the oligos lit-1idel_Fw and lit-1idel_Rv. Deletion of the EFL-3 binding
627 region was confirmed by sequencing.

628 Single-copy woCRE strain was generated with the MosSCI method using animals of the
629 EG8080 strain with a Mos1 transposon insertion on chromosome III (*oxTi444*)[92]. pHIN32
630 was injected at 50 ng/µL together with 50 ng/µL of pCFJ601 (Mos1 transposase), 10 ng/µL
631 of pMA122 (heat-shock-inducible *peel-1* toxin) and and 10 ng/µl, 2.5 ng/µl and 5 ng/µl of
632 the co-injection markers (pGH8, *myo-2::dsRed*, *myo-3::mCherry*). After injection animals
633 were kept at 25°C until they were starved. Heat shock was performed at 33°C for 3.5
634 hours and the plates were allowed to recover for 3 hours at room temperature before
635 'reverse chunking'. The next day the top of the laws on each chunck was screened for
636 normal roaming animals with the absence of co-injection markers. Homozygous lines
637 were confirmed molecularly for the presence of single-copy transgenes using oligos
638 NM3880 and NM3884.

639 **Phenotypic analysis and microscopy**

640 For phenotypic characterisation, animals were anesthetised on 3% agarose pads
641 containing 100 µM sodium azide (NaN_3), secured with a coverslip and visualised under

642 an AxioScope A1 (Zeiss) upright epifluorescence microscope with a LED light source with
643 a RETIGA R6 camera controlled by the Ocular software. Seam cell number was scored
644 in 1 lateral side of early adult animals containing *SCM::GFP* marker. Visualisation of the
645 seam cell membrane was achieved with *wrt-2::GFP::PH; wrt-2::GFP::H2B* markers and
646 animals were scored at 30 hours post-bleaching for late L2 stage, at 40 hours post-
647 bleaching for late L3 stage and 48 hours post-bleaching for late L4 stage.

648 Protein reporter images were acquired using a Leica SP8 Inverted confocal microscope
649 with a x63/1.4 oil DIC objective controlled by LAS X software. Animals were mounted in
650 5% agarose pads containing 100 µM sodium azide (NaN_3) and secured with a coverslip.
651 To visualise L2 symmetric and asymmetric divisions animals were observed at 26 hours
652 post-bleaching. To visualise L3 asymmetric divisions, animals were synchronised by egg
653 laying over a period of 2 hours and observed after 35 hours. Fluorescence intensity for
654 EFL-3::GFP, LIT-1::GFP, EGL-18::mNG and GFP::POP-1 was quantified using FIJI
655 macros developed by the Imperial College FILM facility. Picture editing was performed
656 using straightening tool and stitching macro from FIJI[93].

657 **Single molecule fluorescent in situ hybridisation**

658 Animals were synchronised by bleaching and were fixed at the appropriate stage using
659 4% formaldehyde for 45 minutes and permeabilised with 70% ethanol. Samples were
660 then incubated with a pool of 24-48 oligos labelled with Quasar 670 (Biosearch
661 Technologies, Novato, CA) for 16 hours. Imaging was performed using the x100 objective
662 of an epifluorescence Ti-eclipse microscope (Nikon) and DU-934 CCD-17291 camera
663 (Andor Technology) operated via the Nikon NIS Elements Software. 23 z-stack slices of
664 0.8 µm were acquired for each animal. Spot quantification was performed using MATLAB
665 (MathWorks) as previously described [94]. Z-slices containing spots where max-projected
666 to give a single image, inverted and merged to the GFP channel using ImageJ (NIH). A
667 complete list of the smFISH probes used in this study is provided in Table S3.

668 For DAPI intensity quantification, z-slices were average-projected. DAPI fluorescence
669 intensity was quantified by manually drawing a region of interest around the seam cell
670 nuclei and measurements of average intensity were taken. Three background readings
671 were taken from the area surrounding the seam cells.

672 **Extraction and amplification of methylated DNA**

673 For Nanodam experiments animals were synchronised by bleaching and grown for three
674 generations in *E. coli* dam-/- dcm-/- bacteria (New England Biolabs, C2925). Two
675 biological replicates were grown in parallel for strains carrying the NanoDam transgenes
676 with and without *efl-3:gfp* for C-terminal and N-terminal Dam:GFP-nanobody
677 configurations. Animals were collected after 48 hours, extensively washed x5 in M9 buffer
678 and stored at -20°C. Purification and amplification of methylated DNA was performed as
679 previously described[56]. Extracted gDNA was digested with DpnI and double stranded
680 adaptors were ligated using T4 DNA ligase. Then, DNA fragments were digested with
681 DpnII and amplified using MyTaq polymerase. Amplicons were purified using QIAquick
682 PCR purification kit and adaptors were removed by AlwI digestion followed by another
683 purification. Library preparation and Next Generation Sequencing on an Illumina HiSeq
684 4000 platform was performed by GENEWIZ.

685 **NanoDam signal profiles, peak calling, and gene assignment**

686 FASTQ files representing paired-end reads for each sample and replicate were processed
687 using the damidseq_pipeline (v.1.5.3)[63]. Reads were mapped to the *C. elegans* WBcel235
688 genome assembly using bowtie2 (v.2.4.5) and scores were calculated per GATC fragment
689 of the genome. Pairwise genome-wide $\log_2$(*efl-3-GFP*; *nanobody-dam*/ *nanobody-dam*)
690 calculations were performed from bam files to produce bedGraph signal files that were
691 normalised by quantile normalisation and arithmetically averaged into a single signal
692 profile. Peak calling was performed using the perl script find_peaks (available at
693 https://github.com/owenjm/find_peaks) with FDR < 0.05. Statistically significant peaks
694 were assigned to genes using UROPA [95] with Caenorhabditis_elegans.WBcel235.106.gtf
695 as the genome annotation file. Peaks were assigned to genes when their centre
696 coordinate was positioned up to 5 kb upstream of a gene start site or 2 kb downstream of
697 the end site. Visualisation of signal tracks and other genomic features was performed
698 using Integrative Genomics Viewer (IGV).

699 **Aggregation plots and heatmaps of signal localization**

Signal aggregation plots and peak localisation heatmaps were generated using the SeqPlots GUI application[96]. Signal and peaks were visualised across genes containing peaks up to 5kb upstream of a gene start site or 2 kb downstream of the end site. Genes were plotted as “anchored” features, where the TSS and the TES are fixed in the x axis and the genic sequence is adjusted to a pseudo-length of 2kb. In aggregation plots, signal is averaged in 10bp bins and y axis represents deviations from the average signal across the plotted region (z-scores). In heatmaps, each coloured line represents the position of a statistically significant peak.

Assessment of overlap between statistically significant peaks

To calculate overlapping statistically significant peaks between the C-terminal and N-terminal Dam:GFP-nanobody configurations, BEDTools intersect tool was used[97]. To test whether overlaps where statistically significant, Monte Carlo simulations were performed using OLOGRAM[98].

QUANTIFICATION AND STATISTICAL ANALYSIS

Graphic representation and statistical analysis were performed using R. Error bars used in all graphs represent the standard deviation. Heatmaps represent relative frequency of seam cell defects per cell lineage, which was calculated by dividing the total number of gains or losses in a cell lineage by the total amount of animals analysed. An unpaired t-test or chi-square test was used to evaluate significance as indicated in the figure legends. Results were considered statistically significant when $p < 0.05$. Asterisks in figures indicate corresponding statistical significance as it follows: * $p < 0.05$; ** $p < 0.01$; *** $p < 0.005$; **** $p < 0.001$.

ACKNOWLEDGEMENTS

This work was supported by the Wellcome Trust [219448/Z/19/Z] and a studentship by La Caixa Foundation. We thank Mark Hintze and Dimitris Katsanos for reagents and bioinformatic support. Some strains were provided by the CGC, which is funded by NIH Office of Research Infrastructure Programs (P40 OD010440). We thank Suny Biotech for generating the EFL-3::GFP and LIT-1::GFP strains. We also thank the facility for Imaging

by Light Microscopy (FILM) at Imperial College London, which is part-supported by funding from the Wellcome Trust [104931/Z/14/Z] and the BBSRC [BB/T017929/1].

Data and Materials Availability

All unique/stable reagents generated in this study are available from the Lead Contact without restriction.

The raw NanoDam sequence files and processed signal files have been deposited in the National Center for Biotechnology Information Gene Expression Omnibus under accession number GSE270959.

Contact for Reagent and Resource Sharing

Further information and requests for resources and reagents should be directed to and will be fulfilled by the Lead Contact, Michalis Barkoulas (m.barkoulas@imperial.ac.uk).

COMPETING INTERESTS

The authors declare no competing interests.

References

1. Slack, J.M.W. (2018). The science of stem cells (Blackwell) https://doi.org/10.1002/9781119235293.
2. Morrison, S.J., and Kimble, J. (2006). Asymmetric and symmetric stem-cell divisions in development and cancer. Nature *441*, 1068–1074. https://doi.org/10.1038/nature04956.
3. Bajaj, J., Diaz, E., and Reya, T. (2020). Stem cells in cancer initiation and progression. Journal of Cell Biology *219*, 1–12. https://doi.org/10.1083/jcb.201911053.
4. Joshi, P.M., Riddle, M.R., Djabrayan, N.J.V., and Rothman, J.H. (2010). *Caenorhabditis elegans* as a model for stem cell biology. Developmental Dynamics *239*, 1539–1554. https://doi.org/10.1002/DVDY.22296.
5. Sulston, J.E., and Horvitz, H.R. (1977). Post-embryonic cell lineages of the nematode, *Caenorhabditis elegans*. Dev Biol *56*, 110–156. https://doi.org/10.1016/0012-1606(77)90158-0.
6. Hedgecock, E.M., and White, J.G. (1985). Polyploid Tissues in the Nematode *Caenorhabditis elegans*. Dev Biol *107*, 128–133.

7. Chisholm, A.D., and Hsiao, T.I. (2012). The *Caenorhabditis elegans* epidermis as a model skin. I: Development, patterning, and growth. Wiley Interdiscip Rev Dev Biol *1*, 861–878. https://doi.org/10.1002/wdev.79.
8. Altun, Z.F., and Hall, D.H. (2024). Epithelial system, hypodermis. In WormAtlas.
9. Katsanos, D., Koneru, S.L., Mestek Boukhibar, L., Gritti, N., Ghose, R., Appleford, P.J., Doitsidou, M., Woollard, A., van Zon, J.S., Poole, R.J., et al. (2017). Stochastic loss and gain of symmetric divisions in the *C. elegans* epidermis perturbs robustness of stem cell number. PLoS Biol *15*, 1–31. https://doi.org/10.1371/journal.pbio.2002429.
10. Pani, A.M., and Goldstein, B. (2018). Direct visualization of a native Wnt in vivo reveals that a long-range Wnt gradient forms by extracellular dispersal. Elife *7*, 1–22. https://doi.org/10.7554/eLife.38325.
11. Gleason, J.E., and Eisenmann, D.M. (2010). Wnt signaling controls the stem cell-like asymmetric division of the epithelial seam cells during *C. elegans* larval development. Dev Biol *348*, 58–66. https://doi.org/10.1016/j.ydbio.2010.09.005.
12. Yamamoto, Y., Takeshita, H., and Sawa, H. (2011). Multiple Wnts redundantly control polarity orientation in *Caenorhabditis elegans* epithelial stem cells. PLoS Genet *7*. https://doi.org/10.1371/journal.pgen.1002308.
13. Jackson, B.M., and Eisenmann, D.M. (2012). β-catenin-dependent Wnt signaling in *C. elegans*: Teaching an old dog a new trick. Cold Spring Harb Perspect Biol *4*, 1–18. https://doi.org/10.1101/cshperspect.a007948.
14. Sawa, H., and Korswagen, H.C. (2013). Wnt signaling in *C. elegans*. WormBook, 1–30. https://doi.org/10.1895/wormbook.1.
15. Goldstein, B., Takeshita, H., Mizumoto, K., and Sawa, H. (2006). Wnt signals can function as positional cues in establishing cell polarity. Dev Cell *10*, 391–396. https://doi.org/10.1016/j.devcel.2005.12.016.
16. Green, J.L., Inoue, T., and Sternberg, P.W. (2008). Opposing Wnt Pathways Orient Cell Polarity during Organogenesis. Cell *134*, 646–656. https://doi.org/10.1016/j.cell.2008.06.026.
17. Mizumoto, K., and Sawa, H. (2007). Two βs or not two βs: regulation of asymmetric division by β-catenin. Trends Cell Biol *17*, 465–473. https://doi.org/10.1016/J.TCB.2007.08.004.
18. Baldwin, A.T., and Phillips, B.T. (2014). The tumor suppressor APC differentially regulates multiple β-catenins through the function of axin and CKIα during *C. elegans* asymmetric stem cell divisions. J Cell Sci *127*, 2771–2781. https://doi.org/10.1242/jcs.146514.
19. Mizumoto, K., and Sawa, H. (2007). Cortical β-Catenin and APC Regulate Asymmetric Nuclear β-Catenin Localization during Asymmetric Cell Division in *C. elegans*. Dev Cell *12*, 287–299. https://doi.org/10.1016/j.devcel.2007.01.004.
20. Takeshita, H., and Sawa, H. (2005). Asymmetric cortical and nuclear localizations of WRM-1/β-catenin during asymmetric cell division in *C. elegans*. Genes Dev *19*, 1743–1748. https://doi.org/10.1101/gad.1322805.
21. Sugioka, K., Mizumoto, K., and Sawa, H. (2011). Wnt regulates spindle asymmetry to generate asymmetric nuclear β-catenin in *C. elegans*. Cell *146*, 942–954. https://doi.org/10.1016/j.cell.2011.07.043.

22. Yang, X.D., Karhadkar, T.R., Medina, J., Robertson, S.M., and Lin, R. (2015). β-Catenin-related protein WRM-1 is a multifunctional regulatory subunit of the LIT-1 MAPK complex. Proc Natl Acad Sci U S A *112*, E137–E146. https://doi.org/10.1073/pnas.1416339112.
23. Shin, Yasuda, J., Rocheleau, C.E., Lin, R., Soto, M., Bei, Y., Davis, R.J., and Mello, C.C. (1999). MOM-4, a MAP Kinase Kinase Kinase-Related Protein, Activates WRM-1/LIT-1 Kinase to Transduce Anterior/Posterior Polarity Signals in *C. elegans*. Mol Cell *4*, 275–280.
24. Lo, M.-C., Gay, F., Odom, R., Shi, Y., and Lin, R. (2004). Phosphorylation by the-Catenin/MAPK Complex Promotes 14-3-3-Mediated Nuclear Export of TCF/POP-1 in Signal-Responsive Cells in *C. elegans*. Cell *117*, 95–106.
25. Meneghini, M.D., Ishitani, T., Carter, C.J., Hisamoto, N., Ninomiya-Tsuji, J., Thorpe, C.J., Hamill, D.R., Matsumoto, K., and Bowerman, B. (1999). MAP kinase and Wnt pathways converge to downregulate an HMG-domain repressor in *Caenorhabditis elegans*. Nature *399*, 793–797.
26. Rocheleau, C.E., Yasuda, J., Shin, T.H., Lin, R., Sawa, H., Okano, H., Priess, J.R., Davis, R.J., and Mello, C.C. (1999). WRM-1 Activates the LIT-1 Protein Kinase to Transduce Anterior/Posterior Polarity Signals in *C. elegans*. Cell *97*, 717–726.
27. Yang, X.D., Huang, S., Lo, M.C., Mizumoto, K., Sawa, H., Xu, W., Robertson, S., and Lin, R. (2011). Distinct and mutually inhibitory binding by two divergent β-catenins coordinates TCF levels and activity in *C. elegans*. Development *138*, 4255–4265. https://doi.org/10.1242/dev.069054.
28. Shetty, P., Lo, M.C., Robertson, S.M., and Lin, R. (2005). *C. elegans* TCF protein, POP-1, converts from repressor to activator as a result of Wnt-induced lowering of nuclear levels. Dev Biol *285*, 584–592. https://doi.org/10.1016/j.ydbio.2005.07.008.
29. Huang, S., Shetty, P., Robertson, S.M., and Lin, R. (2007). Binary cell fate specification during *C. elegans* embryogenesis driven by reiterated reciprocal asymmetry of TCF POP-1 and its coactivator β-catenin SYS-1. Development *134*, 2685–2695. https://doi.org/10.1242/dev.008268.
30. Phillips, B.T., III, A.R.K., King, R., Hardin, J., and Kimble, J. (2007). Reciprocal asymmetry of SYS-1/β-catenin and POP-1/TCF controls asymmetric divisions in *Caenorhabditis elegans*. Proc Natl Acad Sci U S A *104*, 3231–3236. https://doi.org/10.1073/pnas.0611507104.
31. Gorrepati, L., Thompson, K.W., and Eisenmann, D.M. (2013). *C. elegans* GATA factors EGL-18 and ELT-6 function downstream of Wnt signaling to maintain the progenitor fate during larval asymmetric divisions of the seam cells. Development (Cambridge) *140*, 2093–2102. https://doi.org/10.1242/dev.091124.
32. Bekas, K.N., and Phillips, B.T. (2022). unc-37/Groucho and lsy-22/AES repress Wnt target genes in *C. elegans* asymmetric cell divisions. bioRxiv, 2022.01.10.475695. https://doi.org/10.1101/2022.01.10.475695.
33. Huang, X., Tian, E., Xu, Y., and Zhang, H. (2009). The *C. elegans* engrailed homolog *ceh-16* regulates the self-renewal expansion division of stem cell-like seam cells. Dev Biol *333*, 337–347. https://doi.org/10.1016/j.ydbio.2009.07.005.

34. Kagoshima, H., Nimmo, R., Saad, N., Tanaka, J., Miwa, Y., Mitani, S., Kohara, Y., and Woollard, A. (2007). The *C. elegans* CBFβ homologue BRO-1 interacts with the Runx factor, RNT-1, to promote stem cell proliferation and self-renewal. Development *134*, 3905–3915. https://doi.org/10.1242/dev.008276.
35. Katsanos, D., and Barkoulas, M. (2022). Targeted DamID in *C. elegans* reveals a direct role for LIN-22 and NHR-25 in antagonizing the epidermal stem cell fate. Sci Adv *8*, 1–16. https://doi.org/10.1126/sciadv.abk3141.
36. Koh, K., and Rothman, J.H. (2001). ELT-5 and ELT-6 are required continuously to regulate epidermal seam cell differentiation and cell fusion in *C. elegans*. Development *128*, 2867–2880.
37. Nimmo, R., and Woollard, A. (2008). Worming out the biology of Runx. Dev Biol *313*, 492–500. https://doi.org/10.1016/j.ydbio.2007.11.002.
38. Smith, J.A., McGarr, P., and Gilleard, J.S. (2005). The *Caenorhabditis elegans* GATA factor elt-1 is essential for differentiation and maintenance of hypodermal seam cells and for normal locomotion. J Cell Sci *118*, 5709–5719. https://doi.org/10.1242/jcs.02678.
39. Xia, D., Zhang, Y., Huang, X., Sun, Y., and Zhang, H. (2007). The *C. elegans* CBFβ homolog, BRO-1, regulates the proliferation, differentiation and specification of the stem cell-like seam cell lineages. Dev Biol *309*, 259–272. https://doi.org/10.1016/j.ydbio.2007.07.020.
40. Attwooll, C., Denchi, E.L., and Helin, K. (2004). The E2F family: Specific functions and overlapping interests. EMBO Journal *23*, 4709–4716. https://doi.org/10.1038/sj.emboj.7600481.
41. Van Den Heuvel, S., and Dyson, N.J. (2008). Conserved functions of the pRB and E2F families. Nat Rev Mol Cell Biol *9*, 713–724. https://doi.org/10.1038/nrm2469.
42. Di Stefano, L., Jensen, M.R., and Helin, K. (2003). E2F7, a novel E2F featuring DP-independent repression of a subset of E2F-regulated genes. EMBO Journal *22*, 6289–6298. https://doi.org/10.1093/emboj/cdg613.
43. Christensen, J., Cloos, P., Toftegaard, U., Klinkenberg, D., Bracken, A.P., Trinh, E., Heeran, M., Di Stefano, L., and Helin, K. (2005). Characterization of E2F8, a novel E2F-like cell-cycle regulated repressor of E2F-activated transcription. Nucleic Acids Res *33*, 5458–5470. https://doi.org/10.1093/NAR/GKI855.
44. Logan, N., Graham, A., Zhao, X., Fisher, R., Maiti, B., Leone, G., and La Thangue, N.B. (2005). E2F-8: An E2F family member with a similar organization of DNA-binding domains to E2F-7. Oncogene *24*, 5000–5004. https://doi.org/10.1038/sj.onc.1208703.
45. De Bruin, A., Maiti, B., Jakoi, L., Timmers, C., Buerki, R., and Leone, G. (2003). Identification and Characterization of E2F7, a Novel Mammalian E2F Family Member Capable of Blocking Cellular Proliferation. Journal of Biological Chemistry *278*, 42041–42049. https://doi.org/10.1074/jbc.M308105200.
46. Lammens, T., Li, J., Leone, G., and De Veylder, L. (2009). Atypical E2Fs: new players in the E2F transcription factor family. Trends Cell Biol *19*, 111–118. https://doi.org/10.1016/j.tcb.2009.01.002.
47. Kent, L.N., and Leone, G. (2019). The broken cycle: E2F dysfunction in cancer. Nat Rev Cancer *19*, 326–338. https://doi.org/10.1038/s41568-019-0143-7.

48. Xie, D., Pei, Q., Li, J., Wan, X., and Ye, T. (2021). Emerging Role of E2F Family in Cancer Stem Cells. Front Oncol *11*. https://doi.org/10.3389/fonc.2021.723137.
49. Cam, H., and Dynlancht, D. (2003). Emerging roles for E2F: Beyond the G1/S transition and DNA replication. Cancer Cell *3*, 311–316.
50. Zalmas, L.P., Zhao, X., Graham, A.L., Fisher, R., Reilly, C., Coutts, A.S., and La Thangue, N.B. (2008). DNA-damage response control of E2F7 and E2F8. EMBO Rep *9*, 252–259. https://doi.org/10.1038/sj.embor.7401158.
51. Chen, Z., and Han, M. (2001). *C. elegans* Rb NuRD and Ras regulate lin-39-mediated cell fusion during vulval fate specification. Current Biology *11*, 1874–1879. https://doi.org/10.1016/S0960-9822(01)00596-6.
52. Page, B.D., Guedes, S., Waring, D., and Priess, J.R. (2001). The *C. elegans* E2F- and DP-related proteins are required for embryonic asymmetry and negatively regulate Ras/MAPK signaling. Mol Cell *7*, 451–460. https://doi.org/10.1016/S1097-2765(01)00193-9.
53. Ceol, C.J., and Horvitz, H.R. (2001). *dpl-1* DP and *efl-1* E2F act with *lin-35* Rb to antagonize Ras signaling in *C. elegans* vulval development. Mol Cell *7*, 461–473. https://doi.org/10.1016/S1097-2765(01)00194-0.
54. Kudron, M., Niu, W., Lu, Z., Wang, G., Gerstein, M., Snyder, M., and Reinke, V. (2013). Tissue-specific direct targets of *Caenorhabditis elegans* Rb/E2F dictate distinct somatic and germline programs. Genome Biol *14*, 1–17. https://doi.org/10.1186/gb-2013-14-1-r5.
55. Schertel, C., and Conradt, B. (2007). *C. elegans* orthologs of components of the RB tumor suppressor complex have distinct pro-apoptotic functions. Development *134*, 3691–3701. https://doi.org/10.1242/dev.004606.
56. Katsanos, D., Ferrando-Marco, M., Razzaq, I., Aughey, G., Southall, T., and Barkoulas, M. (2021). Gene expression profiling of epidermal cell types in *C. elegans* using Targeted-DamID. Development *148*, dev199452. https://doi.org/10.1242/DEV.199452.
57. Winn, J., Carter, M., Avery, L., and Cameron, S. (2011). Hox and a newly identified E2F co-repress cell death in *Caenorhabditis elegans*. Genetics *188*, 897–905. https://doi.org/10.1534/genetics.111.128421.
58. Chen, H.Z., Ouseph, M.M., Li, J., Pécot, T., Chokshi, V., Kent, L., Bae, S., Byrne, M., Duran, C., Comstock, G., et al. (2012). Canonical and atypical E2Fs regulate the mammalian endocycle. Nat Cell Biol *14*, 1192–1202. https://doi.org/10.1038/ncb2595.
59. Pandit, S.K., Westendorp, B., Nantasanti, S., Van Liere, E., Tooten, P.C.J., Cornelissen, P.W.A., Toussaint, M.J.M., Lamers, W.H., and De Bruin, A. (2012). E2F8 is essential for polyploidization in mammalian cells. Nat Cell Biol *14*, 1181–1191. https://doi.org/10.1038/ncb2585.
60. Yee, C., Xiao, Y., Katsanos, D., Medwig-Kinney, T.N., Zhang, W., Shen, K., Matus, D.Q., and Barkoulas, M. (2023). A NanoDam toolkit for tissue-specific transcription factor profiling in *C. elegans*. bioRxiv. https://doi.org/10.1101/2023.05.31.543105.
61. Tang, J.L.Y., Hakes, A.E., Krautz, R., Suzuki, T., Contreras, E.G., Fox, P.M., and Brand, A.H. (2022). NanoDam identifies novel temporal transcription factors

941 conserved between the *Drosophila* central brain and visual system. Dev Cell *57*,
942 1193–1207.
943 62. Southall, T.D., Gold, K.S., Egger, B., Davidson, C.M., Caygill, E.E., Marshall, O.J.,
944 and Brand, A.H. (2013). Cell-type-specific profiling of gene expression and
945 chromatin binding without cell isolation: Assaying RNA pol II occupancy in neural
946 stem cells. Dev Cell *26*, 101–112. https://doi.org/10.1016/j.devcel.2013.05.020.
947 63. Marshall, O.J., and Brand, A.H. (2015). Damidseq-pipeline: An automated pipeline
948 for processing DamID sequencing datasets. Bioinformatics *31*, 3371–3373.
949 https://doi.org/10.1093/bioinformatics/btv386.
950 64. Cao, J., Packer, J.S., Ramani, V., Cusanovich, D.A., Huynh, C., Daza, R., Qiu, X.,
951 Lee, C., Furlan, S.N., Steemers, F.J., et al. (2017). Comprehensive single-cell
952 transcriptional profiling of a multicellular organism. Science (1979) *357*, 661–667.
953 https://doi.org/10.1126/science.aam8940.
954 65. Ashley, G.E., Duong, T., Levenson, M.T., Martinez, M.A.Q., Johnson, L.C.,
955 Hibshman, J.D., Saeger, H.N., Palmisano, N.J., Doonan, R., Martinez-Mendez,
956 R., et al. (2021). An expanded auxin-inducible degron toolkit for *Caenorhabditis*
957 *elegans*. Genetics *217*. https://doi.org/10.1093/genetics/iyab006.
958 66. Coutts, A.S., Munro, S., and La Thangue, N.B. (2018). Functional interplay
959 between E2F7 and ribosomal rRNA gene transcription regulates protein
960 synthesis. Cell Death Dis *9*. https://doi.org/10.1038/s41419-018-0529-6.
961 67. Zalmas, L.P., Coutts, A.S., Helleday, T., and Thangue, N.B.L. (2013). E2F-7
962 couples DNA damage-dependent transcription with the DNA repair process. Cell
963 Cycle *12*, 3037–3051. https://doi.org/10.4161/cc.26078.
964 68. Kipreos, E.T., and van den Heuvel, S. (2019). Developmental control of the cell
965 cycle: Insights from *Caenorhabditis elegans*. Genetics *211*, 797–829.
966 https://doi.org/10.1534/genetics.118.301643.
967 69. Thurlings, I., Martínez-López, L.M., Westendorp, B., Zijp, M., Kuiper, R., Tooten,
968 P., Kent, L.N., Leone, G., Vos, H.J., Burgering, B., et al. (2017). Synergistic
969 functions of E2F7 and E2F8 are critical to suppress stress-induced skin cancer.
970 Oncogene *36*, 829–839. https://doi.org/10.1038/onc.2016.251.
971 70. Park, S.A., Lim, Y.J., Ku, W.L., Zhang, D., Cui, K., Tang, L.Y., Chia, C., Zanvit, P.,
972 Chen, Z., Jin, W., et al. (2022). Opposing functions of circadian protein DBP and
973 atypical E2F family E2F8 in anti-tumor Th9 cell differentiation. Nat Commun *13*.
974 https://doi.org/10.1038/s41467-022-33733-8.
975 71. Segeren, H.A., van Rijnberk, L.M., Moreno, E., Riemers, F.M., van Liere, E.A.,
976 Yuan, R., Wubbolts, R., de Bruin, A., and Westendorp, B. (2020). Excessive E2F
977 Transcription in Single Cancer Cells Precludes Transient Cell-Cycle Exit after
978 DNA Damage. Cell Rep *33*. https://doi.org/10.1016/j.celrep.2020.108449.
979 72. Westendorp, B., Mokry, M., Groot Koerkamp, M.J.A., Holstege, F.C.P., Cuppen,
980 E., and De Bruin, A. (2012). E2F7 represses a network of oscillating cell cycle
981 genes to control S-phase progression. Nucleic Acids Res *40*, 3511–3523.
982 https://doi.org/10.1093/nar/gkr1203.
983 73. Mitxelena, J., Apraiz, A., Vallejo-Rodriguez, J., Malumbres, M., and Zubiaga, A.M.
984 (2016). E2F7 regulates transcription and maturation of multiple microRNAs to
985 restrain cell proliferation. Nucleic Acids Res *44*, 5557–5570.
986 https://doi.org/10.1093/nar/gkw146.

74. Soukup, E.M., Bettinger, J.C., and Mathies, L.D. (2022). Transcription factors regulating the fate and developmental potential of a multipotent progenitor in *Caenorhabditis elegans*. G3: Genes, Genomes, Genetics *12*. https://doi.org/10.1093/g3journal/jkac232.
75. van der Horst, S.E.M., Cravo, J., Woollard, A., Teapal, J., and van den Heuvel, S. (2019). *C. elegans* Runx/CBFβ suppresses POP-1 TCF to convert asymmetric to proliferative division of stem cell-like seam cells. Development *146*, 1–14. https://doi.org/10.1242/dev.180034.
76. Maiti, B., Li, J., De Bruin, A., Gordon, F., Timmers, C., Opavsky, R., Patil, K., Tuttle, J., Cleghorn, W., and Leone, G. (2005). Cloning and characterization of mouse E2F8, a novel mammalian E2F family member capable of blocking cellular proliferation. J Biol Chem *280*, 18211–18220. https://doi.org/10.1074/JBC.M501410200.
77. Van Rijnberk, L.M., Van Der Horst, S.E.M., Van Den Heuvel, S., and Ruijtenberg, S. (2017). A dual transcriptional reporter and CDK-activity sensor marks cell cycle entry and progression in *C. elegans*. PLoS One *12*. https://doi.org/10.1371/journal.pone.0171600.
78. Jin, Y., Anbarchian, T., Wu, P., Sarkar, A., Fish, M., Peng, W.C., and Nusse, R. (2022). Wnt signaling regulates hepatocyte cell division by a transcriptional repressor cascade. PNAS *119*. https://doi.org/10.1073/pnas.
79. Ishitani, T., Ninomiya-Tsuji, J., and Matsumoto, K. (2003). Regulation of Lymphoid Enhancer Factor 1/T-Cell Factor by Mitogen-Activated Protein Kinase-Related Nemo-Like Kinase-Dependent Phosphorylation in Wnt/β-Catenin Signaling. Mol Cell Biol *23*, 1379–1389. https://doi.org/10.1128/mcb.23.4.1379-1389.2003.
80. Ishitani, T., Ninomiya-Tsuji, J., Nagai[2], S.-I., Nishita[2], M., Meneghini[3], M., Barker, N., Watermank, M., Bowerman[3], B., Clevers, H., Shibuya[2], H., et al. (1999). The TAK1±NLK±MAPK-related pathway antagonizes signalling between β-catenin and transcription factor TCF. Nature *399*, 798–802.
81. Ota, S., Ishitani, S., Shimizu, N., Matsumoto, K., Itoh, M., and Ishitani, T. (2012). NLK positively regulates Wnt/β-catenin signalling by phosphorylating LEF1 in neural progenitor cells. EMBO Journal *31*, 1904–1915. https://doi.org/10.1038/emboj.2012.46.
82. Baldwin, A.T., Clemons, A.M., and Phillips, B.T. (2016). Unique and redundant β-catenin regulatory roles of two Dishevelled paralogs during *C. elegans* asymmetric cell division. J Cell Sci *129*, 983–993. https://doi.org/10.1242/jcs.175802.
83. Ren, H., and Zhang, H. (2010). Wnt signaling controls temporal identities of seam cells in *Caenorhabditis elegans*. Dev Biol *345*, 144–155. https://doi.org/10.1016/j.ydbio.2010.07.002.
84. Mallick, A., Ranawade, A., and Gupta, B.P. (2019). Role of PRY-1/Axin in heterochronic miRNA-mediated seam cell development. BMC Dev Biol *19*, 1–12. https://doi.org/10.1186/s12861-019-0197-5.
85. Zhan, T., Rindtorff, N., and Boutros, M. (2017). Wnt signaling in cancer. Oncogene *36*, 1461–1473. https://doi.org/10.1038/onc.2016.304.
86. Zhang, M., Xu, Y., Zhang, Y., and Lou, G. (2023). E2F8 knockdown suppresses cell proliferation and induces cell cycle arrest via Wnt/β-Catenin pathway in

ovarian cancer. Chinese Journal of Physiology *66*, 266–275. https://doi.org/10.4103/cjop.CJOP-D-22-00142.

87. Hughes, T.A., and Brady, H.J.M. (2005). Cross-talk between pRb/E2F and Wnt/β-catenin pathways: E2F1 induces axin2 leading to repression of Wnt signalling and to increased cell death. Exp Cell Res *303*, 32–46. https://doi.org/10.1016/j.yexcr.2004.09.014.
88. Yu, S., Yerges-Armstrong, L.M., Chu, Y., Zmuda, J.M., and Zhang, Y. (2013). E2F1 effects on osteoblast differentiation and mineralization are mediated through up-regulation of frizzled-1. Bone *56*, 234–241. https://doi.org/10.1016/j.bone.2013.06.019.
89. Brenner, S. (1974). The genetics of *Caenorhabditis elegans*. Genetics *77*, 71–94.
90. Kamath, R.S., Fraser, A.G., Dong, Y., Poulin, G., Durbin, R., Gotta, M., Kanapin, A., Le Bot, N., Moreno, S., Sohrmann, M., et al. (2003). Systematic functional analysis of the *Caenorhabditis elegans* genome using RNAi. Nature *421*, 231–237. https://doi.org/10.1038/nature01278.
91. Kamath, R.S., and Ahringer, J. (2003). Genome-wide RNAi screening in *Caenorhabditis elegans*. Methods *30*, 313–321. https://doi.org/10.1016/S1046-2023(03)00050-1.
92. Frøkjær-Jensen, C., Davis, M.W., Sarov, M., Taylor, J., Flibotte, S., LaBella, M., Pozniakovsky, A., Moerman, D.G., and Jorgensen, E.M. (2014). Random and targeted transgene insertion in *Caenorhabditis elegans* using a modified Mos1 transposon. Nat Methods *11*, 529–534. https://doi.org/10.1038/nmeth.2889.
93. Preibisch, S., Saalfeld, S., and Tomancak, P. (2009). Globally optimal stitching of tiled 3D microscopic image acquisitions. Bioinformatics *25*, 1463–1465. https://doi.org/10.1093/bioinformatics/btp184.
94. Raj, A., van den Bogaard, P., Rifkin, S.A., van Oudenaarden, A., and Tyagi, S. (2008). Imaging individual mRNA molecules using multiple singly labelled probes. Nat Methods *5*, 877–879. https://doi.org/10.1038/nmeth.1253.
95. Kondili, M., Fust, A., Preussner, J., Kuenne, C., Braun, T., and Looso, M. (2017). UROPA: A tool for Universal RObust Peak Annotation. Sci Rep *7*. https://doi.org/10.1038/s41598-017-02464-y.
96. Stempor, P., and Ahringer, J. (2016). SeqPlots - Interactive software for exploratory data analyses, pattern discovery and visualization in genomics. Wellcome Open Res *1*. https://doi.org/10.12688/WELLCOMEOPENRES.10004.1.
97. Quinlan, A.R., and Hall, I.M. (2010). BEDTools: a flexible suite of utilities for comparing genomic features. Bioinformatics *26*, 841–842. https://doi.org/10.1093/BIOINFORMATICS/BTQ033.
98. Ferré, Q., Charbonnier, G., Sadouni, N., Lopez, F., Kermezli, Y., Spicuglia, S., Capponi, C., Ghattas, B., and Puthier, D. (2019). OLOGRAM: Determining significance of total overlap length between genomic regions sets. Bioinformatics *36*, 1920–1922. https://doi.org/10.1093/BIOINFORMATICS/BTZ810.

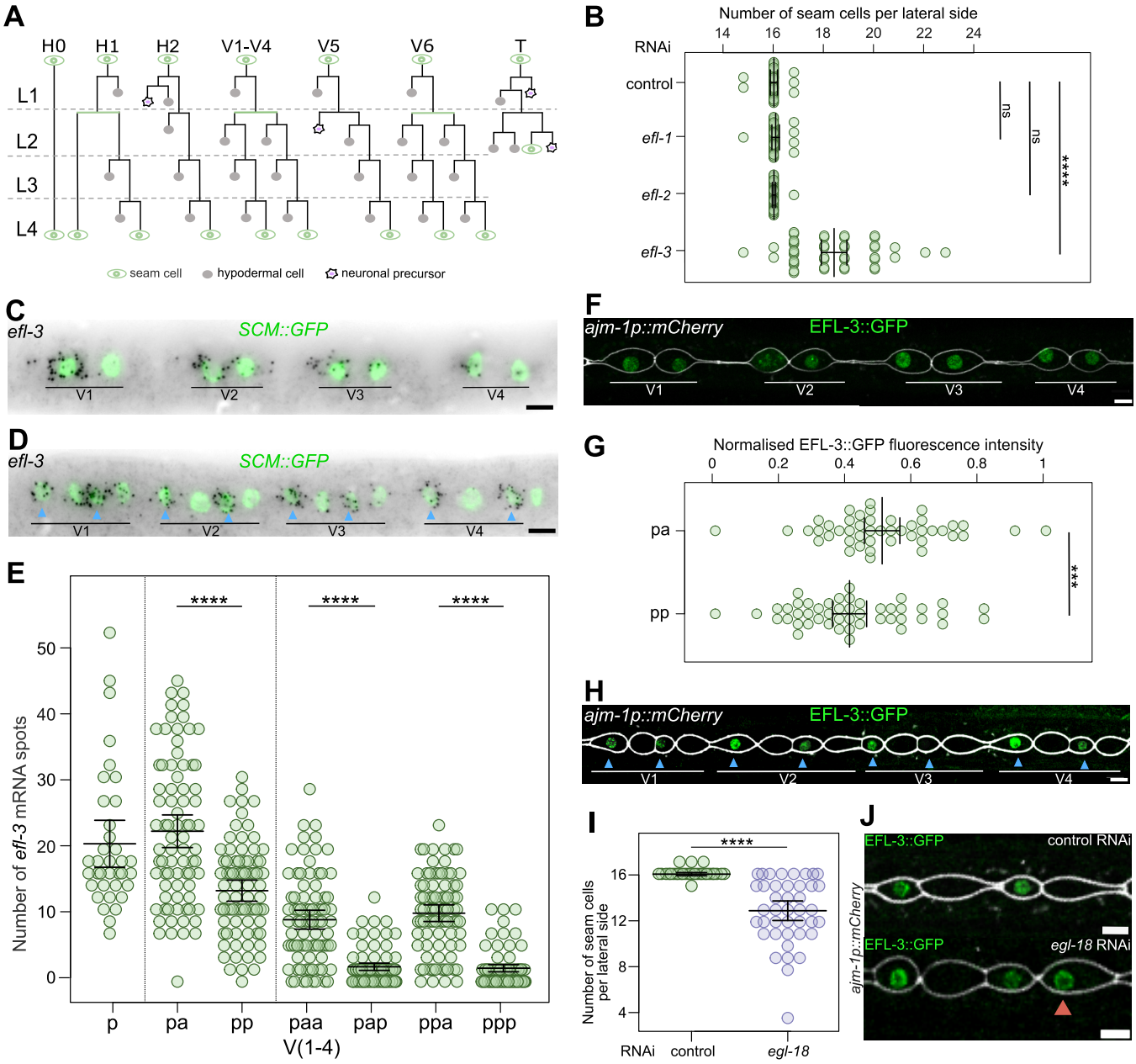
A
H0
H1
H2
V1-V4
V5
V6
T
L1
L2
L3
L4
seam cell
hypodermal cell
neuronal precursor
B
Number of seam cells per lateral side
RNAi
control
efl-1
efl-2
efl-3
ns
ns
****
C
efl-3
SCM::GFP
V1
V2
V3
V4
D
efl-3
SCM::GFP
V1
V2
V3
V4
E
Number of efl-3 mRNA spots
****
****
****
p
pa
pp
paa
pap
ppa
ppp
V(1-4)
F
ajm-1p::mCherry
EFL-3::GFP
V1
V2
V3
V4
G
Normalised EFL-3::GFP fluorescence intensity
pa
pp
***
H
ajm-1p::mCherry
EFL-3::GFP
V1
V2
V3
V4
I
Number of seam cells per lateral side
****
RNAi
control
egl-18
J
EFL-3::GFP
control RNAi
ajm-1p::mCherry
EFL-3::GFP
egl-18 RNAi

Figure 1

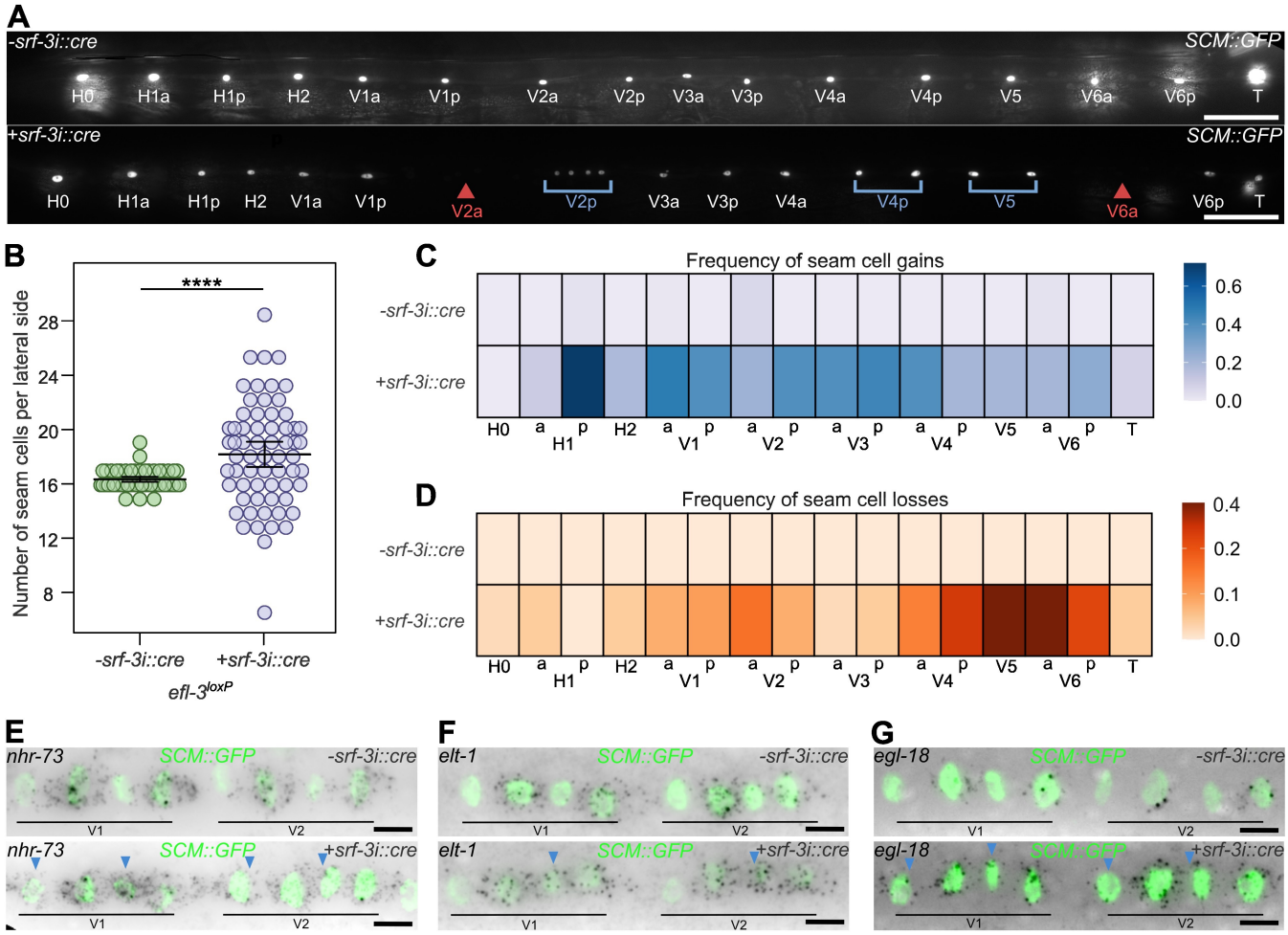
A
-srf-3i::cre
SCM::GFP
H0 H1a H1p H2 V1a V1p V2a V2p V3a V3p V4a V4p V5 V6a V6p T
+srf-3i::cre
SCM::GFP
H0 H1a H1p H2 V1a V1p V2a V2p V3a V3p V4a V4p V5 V6a V6p T
B
****
Number of seam cells per lateral side
28
24
20
16
12
8
-srf-3i::cre
+srf-3i::cre
efl-3loxP
C
Frequency of seam cell gains
-srf-3i::cre
+srf-3i::cre
H0 a p H1 H2 a p V1 a p V2 a p V3 a p V4 V5 a p V6 T
0.6
0.4
0.2
0.0
D
Frequency of seam cell losses
-srf-3i::cre
+srf-3i::cre
H0 a p H1 H2 a p V1 a p V2 a p V3 a p V4 V5 a p V6 T
0.4
0.2
0.1
0.0
E
nhr-73
SCM::GFP
-srf-3i::cre
V1
V2
nhr-73
SCM::GFP
+srf-3i::cre
V1
V2
F
elt-1
SCM::GFP
-srf-3i::cre
V1
V2
elt-1
SCM::GFP
+srf-3i::cre
V1
V2
G
egl-18
SCM::GFP
-srf-3i::cre
V1
V2
egl-18
SCM::GFP
+srf-3i::cre
V1
V2

Figure 2

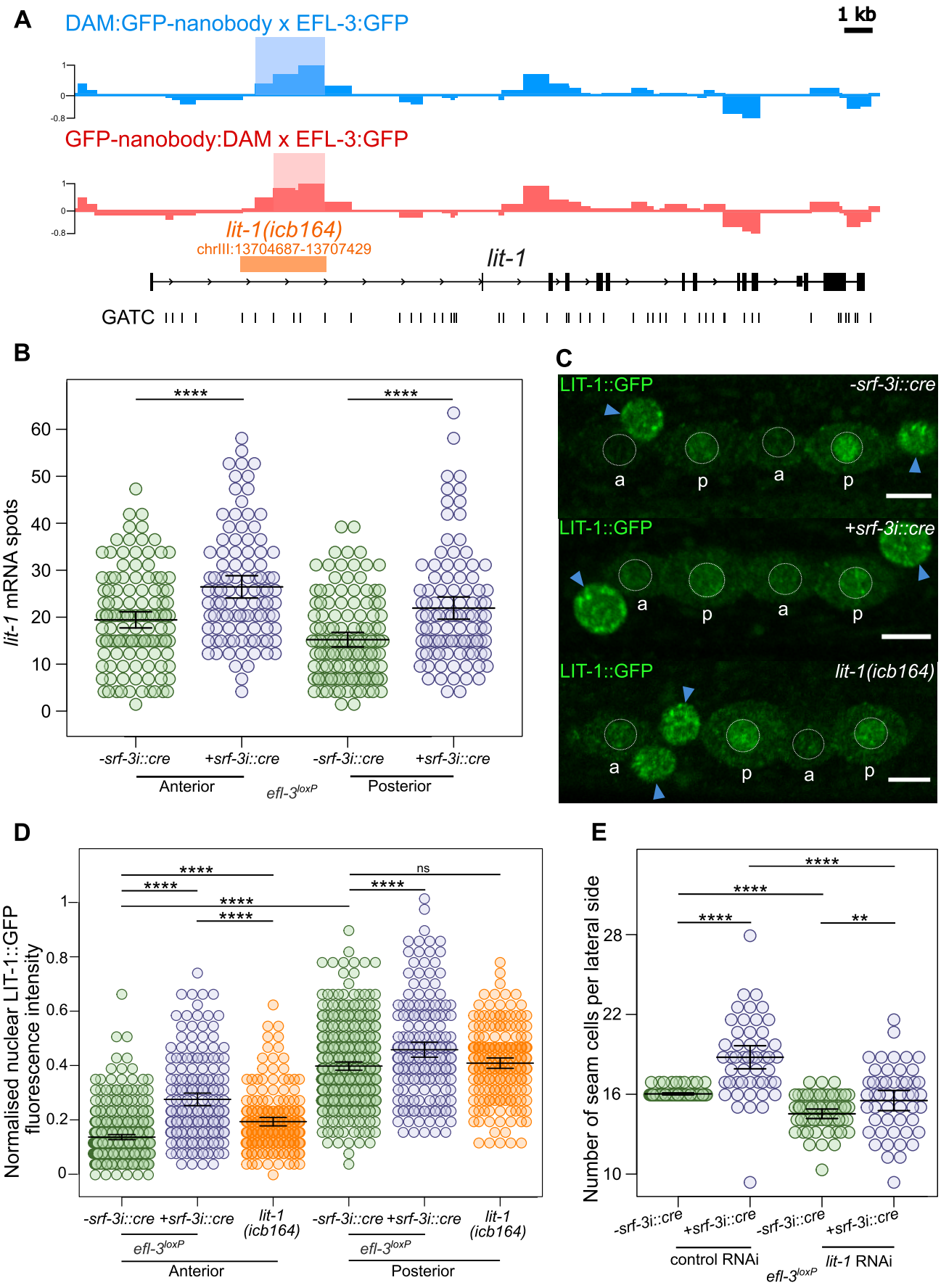
A
DAM:GFP-nanobody x EFL-3:GFP
1 kb
GFP-nanobody:DAM x EFL-3:GFP
lit-1(icb164)
chrIII:13704687-13707429
lit-1
GATC
B
lit-1 mRNA spots
-srf-3i::cre
+srf-3i::cre
Anterior
Posterior
efl-3loxP
C
LIT-1::GFP
-srf-3i::cre
+srf-3i::cre
lit-1(icb164)
a
p
D
Normalised nuclear LIT-1::GFP fluorescence intensity
lit-1 (icb164)
ns
E
Number of seam cells per lateral side
control RNAi
lit-1 RNAi

Figure 3

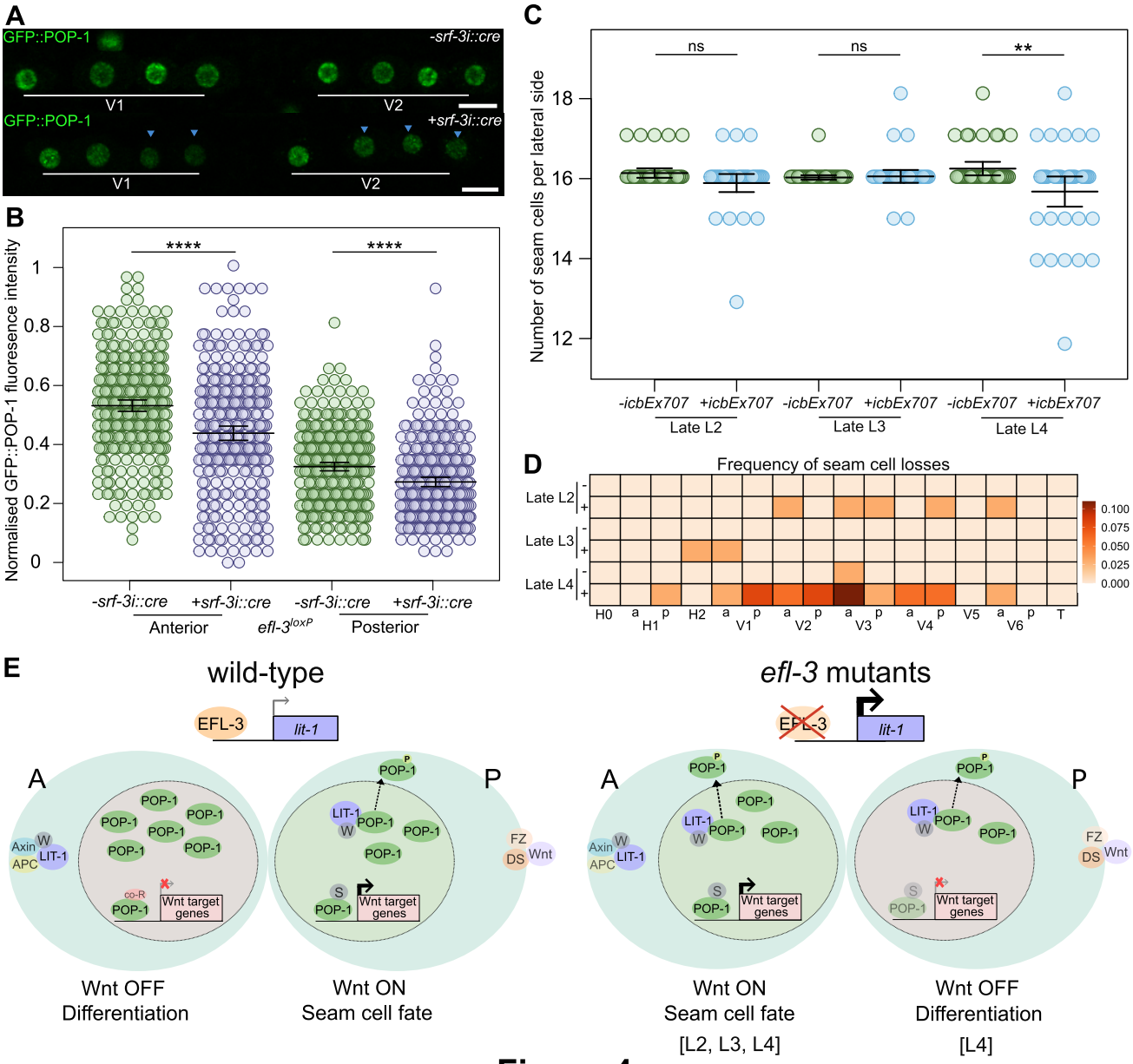
A
GFP::POP-1
-srf-3i::cre
V1
V2
GFP::POP-1
+srf-3i::cre
V1
V2
B
Normalised GFP::POP-1 fluoresence intensity
****
****
-srf-3i::cre
+srf-3i::cre
-srf-3i::cre
+srf-3i::cre
Anterior
efl-3loxP
Posterior
C
Number of seam cells per lateral side
ns
ns
**
-icbEx707
+icbEx707
Late L2
Late L3
Late L4
D
Frequency of seam cell losses
Late L2
Late L3
Late L4
0.100
0.075
0.050
0.025
0.000
E
wild-type
EFL-3
lit-1
A
P
POP-1
LIT-1
Axin
APC
W
co-R
Wnt target genes
FZ
DS
Wnt
Wnt OFF
Differentiation
Wnt ON
Seam cell fate
efl-3 mutants
Wnt ON
Seam cell fate
[L2, L3, L4]
Wnt OFF
Differentiation
[L4]

Figure 4

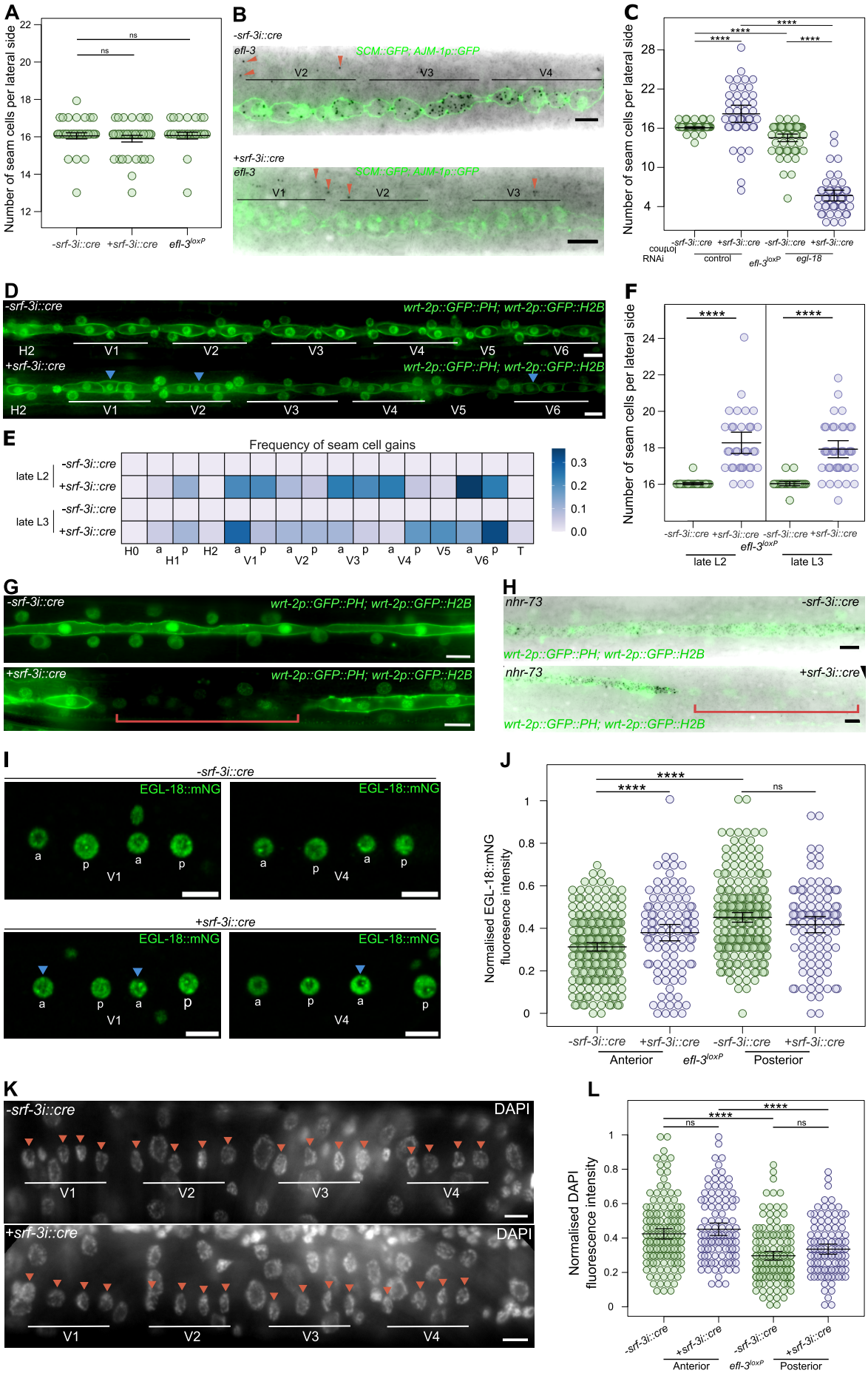
A
Number of seam cells per lateral side
ns
ns
-srf-3i::cre
+srf-3i::cre
efl-3loxP
B
-srf-3i::cre
efl-3
SCM::GFP; AJM-1p::GFP
V2
V3
V4
+srf-3i::cre
efl-3
SCM::GFP; AJM-1p::GFP
V1
V2
V3
C
Number of seam cells per lateral side
control RNAi
control
efl-3loxP
egl-18
D
-srf-3i::cre
wrt-2p::GFP::PH; wrt-2p::GFP::H2B
H2
V1
V2
V3
V4
V5
V6
+srf-3i::cre
wrt-2p::GFP::PH; wrt-2p::GFP::H2B
E
Frequency of seam cell gains
late L2
late L3
-srf-3i::cre
+srf-3i::cre
H0
H1
H2
V1
V2
V3
V4
V5
V6
T
F
Number of seam cells per lateral side
late L2
late L3
efl-3loxP
G
-srf-3i::cre
wrt-2p::GFP::PH; wrt-2p::GFP::H2B
+srf-3i::cre
wrt-2p::GFP::PH; wrt-2p::GFP::H2B
H
nhr-73
-srf-3i::cre
wrt-2p::GFP::PH; wrt-2p::GFP::H2B
nhr-73
+srf-3i::cre
wrt-2p::GFP::PH; wrt-2p::GFP::H2B
I
-srf-3i::cre
EGL-18::mNG
V1
V4
+srf-3i::cre
EGL-18::mNG
V1
V4
J
Normalised EGL-18::mNG fluoresence intensity
Anterior
efl-3loxP
Posterior
K
-srf-3i::cre
DAPI
V1
V2
V3
V4
+srf-3i::cre
DAPI
V1
V2
V3
V4
L
Normalised DAPI fluorescence intensity
Anterior
efl-3loxP
Posterior

Figure S1

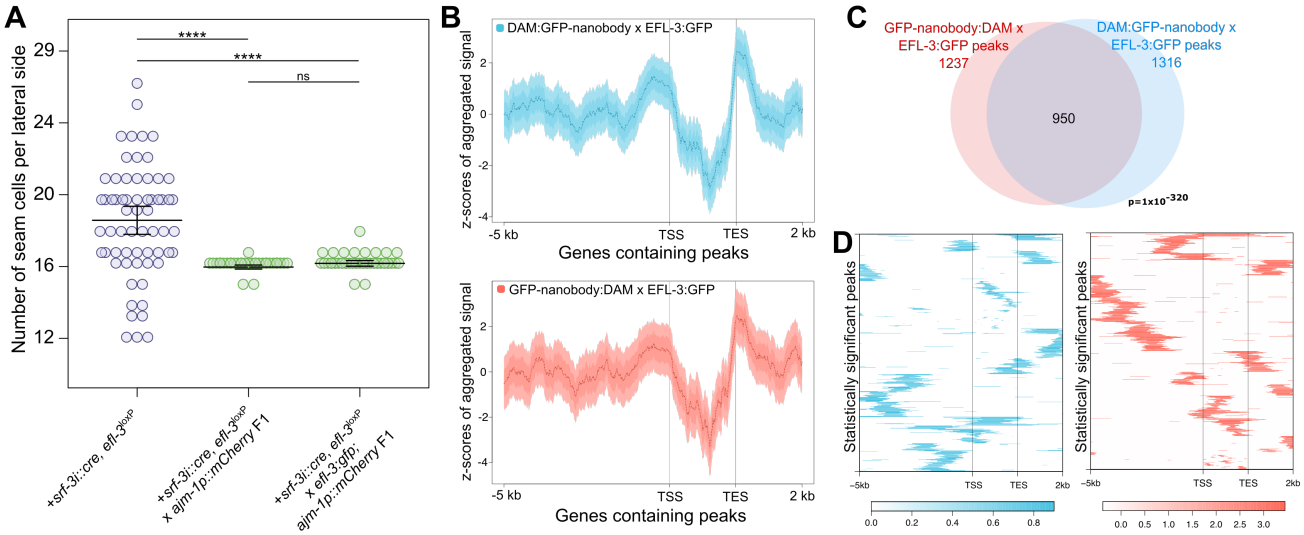
A
Number of seam cells per lateral side
29
24
20
16
12
****
****
ns
+srf-3i::cre, efl-3loxP
+srf-3i::cre, efl-3loxP x ajm-1p::mCherry F1
+srf-3i::cre, efl-3loxP x efl-3:gfp; ajm-1p::mCherry F1
B
DAM:GFP-nanobody x EFL-3:GFP
z-scores of aggregated signal
-5 kb
TSS
TES
2 kb
Genes containing peaks
GFP-nanobody:DAM x EFL-3:GFP
z-scores of aggregated signal
-5 kb
TSS
TES
2 kb
Genes containing peaks
C
GFP-nanobody:DAM x EFL-3:GFP peaks 1237
DAM:GFP-nanobody x EFL-3:GFP peaks 1316
950
p=1x10-320
D
Statistically significant peaks
-5kb
TSS
TES
2kb
0.0
0.2
0.4
0.6
0.8
Statistically significant peaks
-5kb
TSS
TES
2kb
0.0
0.5
1.0
1.5
2.0
2.5
3.0

Figure S2

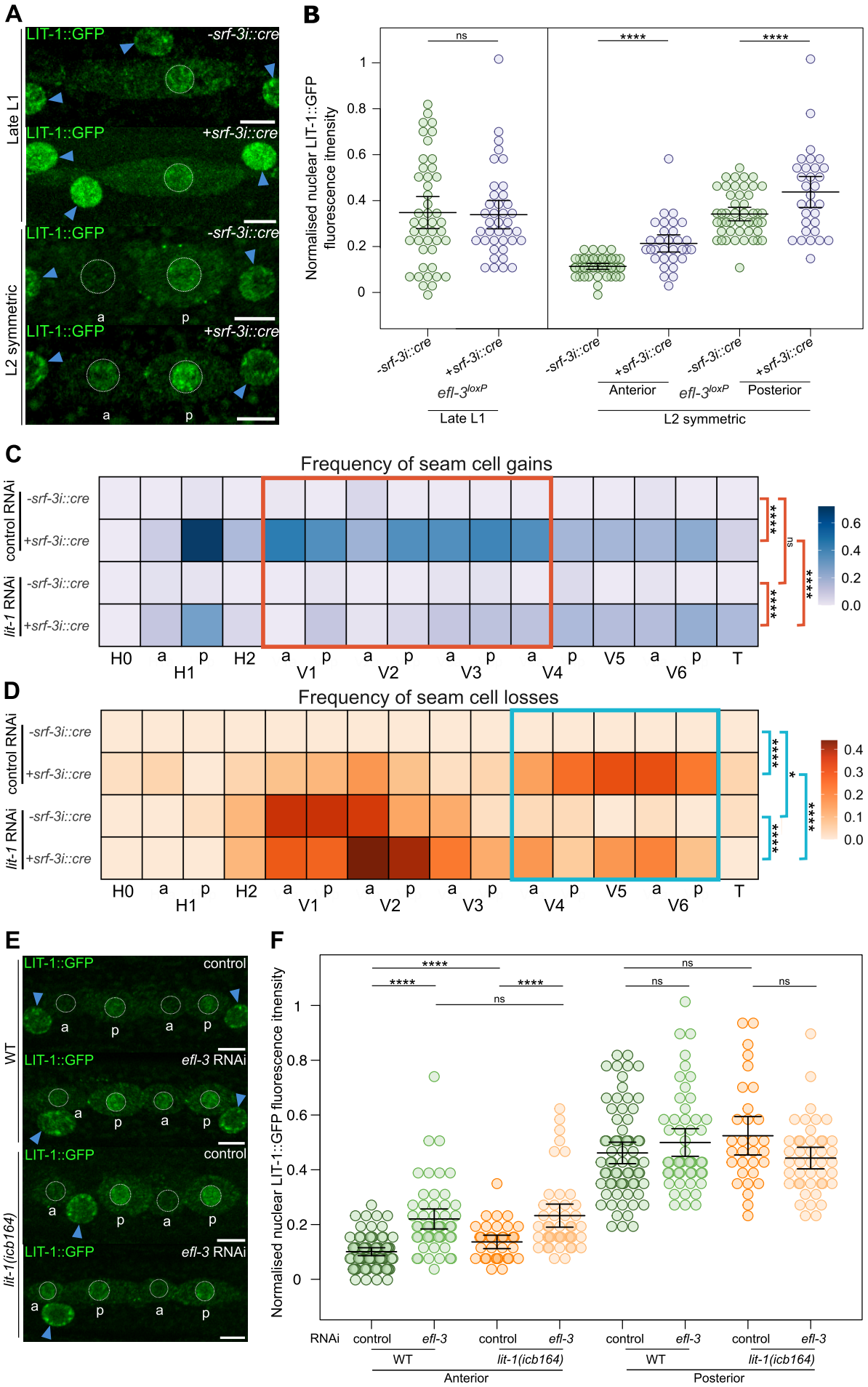
A
LIT-1::GFP
-srf-3i::cre
+srf-3i::cre
Late L1
L2 symmetric
a
p
B
Normalised nuclear LIT-1::GFP fluorescence itnensity
ns
****
-srf-3i::cre
+srf-3i::cre
efl-3loxP
Late L1
Anterior
Posterior
L2 symmetric
C
Frequency of seam cell gains
control RNAi
lit-1 RNAi
H0
H1
H2
V1
V2
V3
V4
V5
V6
T
D
Frequency of seam cell losses
E
control
efl-3 RNAi
WT
lit-1(icb164)
F
Normalised nuclear LIT-1::GFP fluorescence itnensity
RNAi
control
efl-3
WT
lit-1(icb164)
Anterior
Posterior

Figure S3

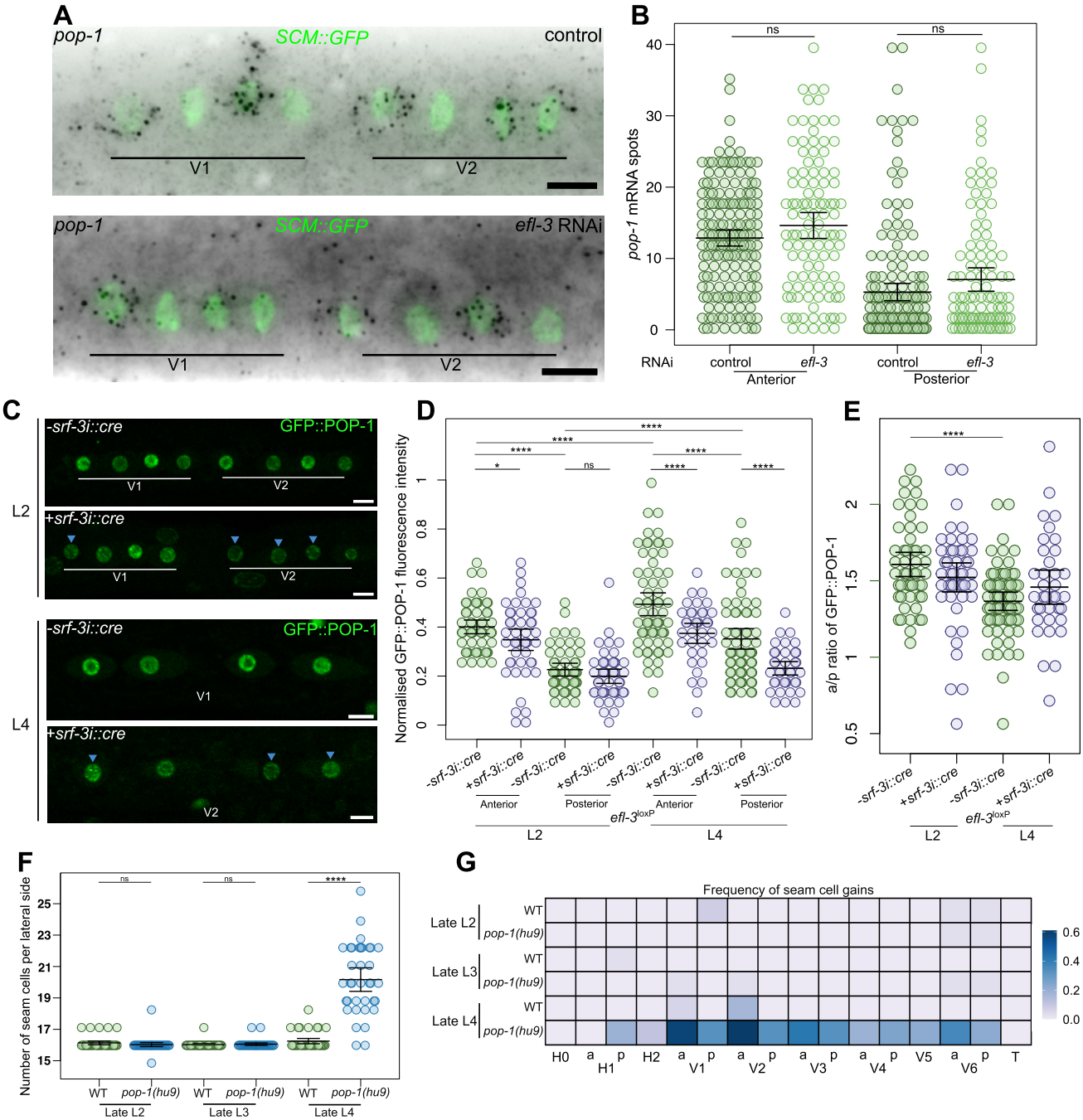
A
pop-1
SCM::GFP
control
V1
V2
pop-1
SCM::GFP
efl-3 RNAi
V1
V2
B
pop-1 mRNA spots
ns
ns
RNAi
control
efl-3
control
efl-3
Anterior
Posterior
C
-srf-3i::cre
GFP::POP-1
+srf-3i::cre
L2
L4
V1
V2
D
Normalised GFP::POP-1 fluorescence intensity
-srf-3i::cre
+srf-3i::cre
Anterior
Posterior
efl-3loxP
L2
L4
E
a/p ratio of GFP::POP-1
-srf-3i::cre
+srf-3i::cre
efl-3loxP
L2
L4
F
Number of seam cells per lateral side
ns
ns
****
WT
pop-1(hu9)
Late L2
Late L3
Late L4
G
Frequency of seam cell gains
Late L2
Late L3
Late L4
WT
pop-1(hu9)
H0
H1
H2
V1
V2
V3
V4
V5
V6
T

Figure S4